UPPSALA
UNIVERSITET

Digital Comprehensive Summaries of Uppsala Dissertations from the Faculty of Science and Technology 1468

Geophysical studies in the western part of the Siljan Ring Impact Crater

HARBE MUHAMAD

ACTA
UNIVERSITATIS
UPSALIENSIS
UPPSALA
2017

ISSN 1651-6214
ISBN 978-91-554-9794-1
urn:nbn:se:uu:diva-312022

Dissertation presented at Uppsala University to be publicly examined in Hamberg, Geocentrum, Villavagen 16, Uppsala, Friday, 3 March 2017 at 10:00 for the degree of Doctor of Philosophy. The examination will be conducted in English. Faculty examiner: Professor Lars Nilsen (Department of Geosciences and Natural Resource Management, Section of Geology, university of Copenhagen, Danmark).

Abstract
Muhamad, H. 2017. Geophysical studies in the western part of the Siljan Ring Impact Crater. *Digital Comprehensive Summaries of Uppsala Dissertations from the Faculty of Science and Technology* 1468. 69 pp. Uppsala: Acta Universitatis Upsaliensis. ISBN 978-91-554-9794-1.

This thesis utilizes several geophysical methods to study the Siljan Ring impact structure, focusing on the western part of the structure. This thesis, and the three papers upon which it is based, reports on attempts to delineate the Paleozoic rocks at depth within the annular ring graben and characterize their structure. In addition, the nature of the basement, which underlies these sedimentary rocks is investigated.

Papers I and III focus on analysis of the down-hole logging and borehole core data. As well as the acquisition, processing and interpretation of 2D high-resolution reflection seismic data from the Mora area. The borehole log responses were compared with the core lithology from the Mora 001 borehole and information from two other cores (Mora VM 2 and Mora MV 3) in order to interpret the logs. The logs reveal significant changes in the lithology between boreholes, indicating a very high level of structural complexity, which is attributed to impact tectonics. In addition, the log data revealed a high sonic velocity contrast between the Silurian and Ordovician successions and a higher apparent temperature gradient than in the northern part of the structure. The interpretation of the high-resolution 2D seismic data suggest that the Mora area has been significantly affected by the impact. Several potential faults were identified in the area and interpreted to be post depositional and related to the impact. In paper II, a 2D seismic profile from the Orsa area (12 km) located in the northwestern part of the Siljan Ring was re-processed. To compliment this seismic line, first break traveltime tomography results, vintage seismic OPAB profiles, new and pre-existing gravity data, aeromagnetic data and the bedrock geological map were used to present a geological model along the Orsa profile. Reprocessing of the seismic data resulted in improved stacked and migrated sections and better imaging of the top of the crystalline basement than the original processing. Integrated interpretation of the seismic profiles suggests that the area has been significantly affected by faulting and that the depth to the basement varies greatly along the different profiles.

Keywords: Siljan ring impact structure, Seismic reflection, Down-hole logging, Gravity, Magnetic, Tomography, Paleozoic rocks

Harbe Muhamad, Department of Earth Sciences, Geophysics, Villav. 16, Uppsala University, SE-75236 Uppsala, Sweden.

ISSN 1651-6214
ISBN 978-91-554-9794-1
urn:nbn:se:uu:diva-312022 (http://urn.kb.se/resolve?urn=urn:nbn:se:uu:diva-312022)

Dedicated to
My beloved Rangeen and
My lovely daughters Laveen & Nivin

List of Papers

This thesis is based on the following papers, which are referred to in the text by their Roman numerals.

I **Muhamad, H.**, Juhlin, C., Lehnert, O., Meinhold, G., Andersson, M., Garcia Juanatey, M., Malehmir, A. (2015) Analysis of borehole geophysical data from the Mora area of the Siljan Ring impact structure, central Sweden. *Journal of Applied Geophysics*, 115:183–196

II **Muhamad, H.**, Juhlin, C., Malehmir, A., Sopher, D. (2016) Integrated interpretation of geophysical data of the Paleozoic structure in the northwestern part of the Siljan Ring impact crater, central Sweden. *Journal of Applied Geophysics*, manuscript under review

III **Muhamad, H.**, Juhlin, C., Sopher, D., Lehnert, O., Meinhold, G., Arslan, A. (2017) High-resolution seismic imaging of Paleozoic rocks in the Mora area, Siljan Ring structure, central Sweden. *GFF,* manuscript under review

Reprints were made with permission from the respective publishers.

Contributions

The papers included in this thesis are the result of collaboration with several authors. The individual contributions of the author of this thesis are summarized.

I The geophysical well data were acquired by myself and one other co-author. I performed the processing and analysis of the downhole logging data. I performed the density measurements in the rock physics laboratory. My main supervisor helped with the elastic finite difference modeling. The interpretation of the data was done in collaboration with my co-authors. I wrote the first draft of the paper, which was later improved by my co-authors.

II I reprocessed the Orsa seismic profile (12 km) and participated in the gravity survey along the Orsa profile. I performed the 3D travel time tomography using the PStomo-eq algorithm (Tryggvason et al., 2002). I performed the processing, analysis and 2.5D modeling of the potential field data. The interpretation of the data was done in collaboration with my co-authors. I wrote the first draft of the paper, which was improved by my co-authors.

III I participated in the seismic data acquisition. I performed the processing and analysis of the seismic data with advice from my main supervisor. I collected the gravity data along seismic line 2 and 42 core samples from the Mora VM-2 borehole with help from my two co-workers. I prepared the samples for laboratory measurements and performed the petrophysical measurements. I generated the synthetic seismogram for the Mora VM-2 borehole. The gravity data processing, analysis and 2.5D modeling were performed by myself. The interpretation of the data was done in collaboration with my co-authors. The first draft of the paper was written by me and later improved by my co-authors.

Contents

Abbreviations

1C	One component
1D	One-dimensional
2.5D	Two-and-half-dimensional
2D	Two-dimensional
3C	Three component
3D	Three-dimensional
CDP	Common depth point
cm	Centimeter
cm^3	Cubic centimeter
DMO	Dip moveout
ELTG	Electric log sonde
g	Gram
Ga	A billion years (Gigayears) ago
GPS	Global positioning system
Hz	Hertz
kg	Kilogram
km	Kilometer
m	Meter
m^3	Cubic meter
Ma	Million years
MEMS	Micro-electro mechanical system
MHz	Megahertz
ms	Millisecond
NMO	Normal moveout
OPAB	Swedish oil prospecting company (Olieprospektering AB)
s	Second
S/N	Signal-to-noise ratio
SGU	Geological Survey of Sweden
TCD	Temperature log sonde
TRSG	Three receiver sonic sonde

1 Introduction

Meteorite impact structures are found on all planetary bodies in the Solar System with a solid surface. On the Earth, there are 190 confirmed impact structures, which have been documented to date (Earth Impact Database, Accessed: 12th Jan. 2017) and this number is increasing each year. An impact crater is an approximately circular depression on the surface of the Earth, formed by the hypervelocity impact of a smaller body. The crater diameter is a key delimiter in the morphology of impact craters. Based on differences in crater diameter we can classify impact structures into two types, simple structures and complex structures. A simple impact crater is bowl-shaped with no interior structure. Complex impact structures generally have a structurally complex rim, a down-faulted annular trough, and an uplifted central area. The impact crater forming process has been divided, somewhat arbitrarily, into three main stages (Gault et al., 1968) (Fig. 1.1): (1) The so-called "contact and compression stage" is when the projectile makes contact with the surface of the Earth, (2) The "excavation stage" occurs directly after the contact and compression stage, when the actual crater is exposed by interactions of the expanding shock wave and the surface, (3) The "modification stage" is the third stage of crater formation. The effects of this stage are governed by the size of transient cavity and the target rock lithologies. If the transient cavity is < 2 - 4 km it undergoes only minor modification, creating a simple bowl shaped crater. If the transient cavity is > 2 - 4 km it undergoes unstable modification controlled by gravity, creating a complex impact crater (Dence, 1965). Impact structure studies are important for two reasons, the first is from a scientific point where we can gain further insight into the impact mechanical process, and in the case of Siljan, also gain an understanding of the paleoenviroment, paleoclimate and paleobiology before the impact occurred. The second reason is due to the economic potential (e.g. Masaitis, 1989; Grieve and Masaitis, 1994; Westbroek and Stewart, 1996; Reimold et al., 2005b), where impact craters have been essential in the formation or hosting of hydrocarbon and mineral deposits.

The crater formation process leads to a sudden increased in temperature and pressure immediately after the impact, which gives rise to partial melting (pseudo-tachylite breccia), fracturing and shatter cone structures, disruption and structural redistribution of geological materials over a very short time period. Major differences between impact events and other geological processes include: (1) the approximate physical conditions that produce shock-deformation effects in the rocks, (2) the concentrated nature of the energy release

at a single point on the Earth's surface, (3) the virtually instantaneous nature of the impact process, and (4) the high strain rates involved (French, 1998).

The Siljan Ring impact structure is the largest known impact structures in Europe (Fig. 1.2). It is located in central Sweden (N 61^{o} 2', E 14^{o} 52') and is Late Devonian in age. The Siljan Ring structure is considered a complex structure. The pre-erosional diameter was estimated to be 52 km based on seismic studies (Grieve, 1988; Juhlin and Pedersen, 1993) and estimated to be 65 km based on the distribution of fractures in the crystalline bedrock interpreted as impact related (Kenkmann and von Dalwigk, 2000a). The geomorphological data suggest that the final diameter is 75 km (Henkel and Aaro, 2005) and the greatest diameter suggested in the literature is 90 km (Holm et al., 2011). The Siljan Ring structure consists of a central uplift that is about 20-30 km wide, this is surrounded by a ring-shaped depression (Juhlin and Pedersen, 1987) filled by Lower Paleozoic rocks that were preserved from post-impact erosion.

In the early 1980s, The Deep Gas Project conducted by the Swedish State Power Board (Vattenfall) attempted to evaluate the potential for abiogenic gas production in the Siljan Ring impact structure (Donofrio et al., 1984; Boden and Eriksson, 1988). This led to a large research project and the acquisition of nine seismic reflection profiles across the structure with a total length about 80 km. These seismic profiles were located in the central, north, northwestern and eastern parts of the structure. In addition, several shallow cored boreholes (~ 400-600 m depth) and two deep boreholes were drilled within the crystalline rocks. The Gravberg-1 borehole (about 6.8 km deep) was drilled in the northern part and the Stenberg-1 borehole (about 6.5 km deep) in the central part (Fig. 1.2). The seismic data results show that the felsic rocks appear to be seismically transparent with a few high amplitude sub-horizontal reflections. Based on the comparison with the borehole lithologies, these high amplitude reflections are interpreted to be generated by thin dolerite sills (5-50 m) within the felsic rocks (Juhlin, 1990; Papasikas and Juhlin, 1997).

In western part of the Siljan Ring two seismic reflection profiles (the Mora and Orsa profiles) were acquired in 2011 (Juhlin et al., 2012) (Fig. 1.2). The objective of these profiles was to map the thicknesses of the Paleozoic rocks in the ring formed depression. Results from these profiles show a complex and discontinuous reflection pattern with significant faulting, especially along the Mora profile (Juhlin at el., 2012).

This thesis utilizes several geophysical methods to study the Siljan Ring impact structure, focusing on the northwestern and southwestern parts of the structure (Fig. 1.2). This thesis, and the three papers upon which it is based, reports on attempts to map the Paleozoic rocks within the annular ring graben and characterize their structure. In addition, the nature of the basement, which underlies these sedimentary rocks, is investigated. In order to do this several different geophysical methods, including seismic reflection, well logging, tomography and potential field data methods, are utilized and their data analyzed

together to give an integrated interpretation. This dissertation is a comprehensive summary of three papers and consists of six chapters. The first chapter provides an introduction and background to the study area. The second chapter presents the geological setting of the Siljan Ring impact structure. The geophysical methods which were used in this study are summarized in chapter three. The main part of the study is presented in chapter four, which contains the summaries of the three papers that the thesis is based upon. This is followed by conclusions and outlook in chapter 5 and finally a summary in Swedish in chapter 6.

Paper I describes geophysical logs, which were acquired in four boreholes in the Mora area located on southwestern side of the Siljan Ring. Three different logs were used to determine the physical properties of the Paleozoic and crystalline rocks in the area (temperature, sonic velocity and electrical resistivity logs). The results from theses logs were interpreted in a lithological context based on correlation with core data from the nearby Mora 001 borehole. In addition, the sonic velocity log from the Mora 001 borehole was used to generate a synthetic seismogram to compare with seismic reflection data acquired further to the north (Mora seismic profile).

Paper II describes reprocessing of the Orsa seismic profile (12 km long), located in northwestern part of the Siljan Ring structure. These data were acquired in 2011 and were reprocessed using additional processing steps relative to the original processing, including a cross-dip correction and dip-moveout corrections (DMO). This reprocessed data along with results from first break traveltime tomography and a set of vintage seismic profiles from the 1970s (OPAB data) are combined with new and pre-existing gravity data, aeromagnetic data and potential field data modeling results to constrain the nature of the Paleozoic structure and uppermost crystalline rocks.

Paper III describes results from four high-resolution 2D seismic reflection profiles, acquired in the Mora area. The seismic data acquisition was carried out using 3C MEMS-based sensors incorporated into a seismic land streamer system and combined with data from wireless recorders deployed in the area. Petrophysical measurements from rock samples collected form the Mora VM-2 core were used to generate a synthetic seismogram to tie with the seismic data. In addition, 13 ground gravity stations were measured along Line 2 and merged with pre-existing data. 2.5D gravity forward modeling was carried out to generate a density model along the line, which produces an anomaly that matches the data. The well log data highlight the extreme structural complexity of the sedimentary succession in this area. Here we use the seismic data to define several fault blocks and to characterize the differing levels of deformation within.

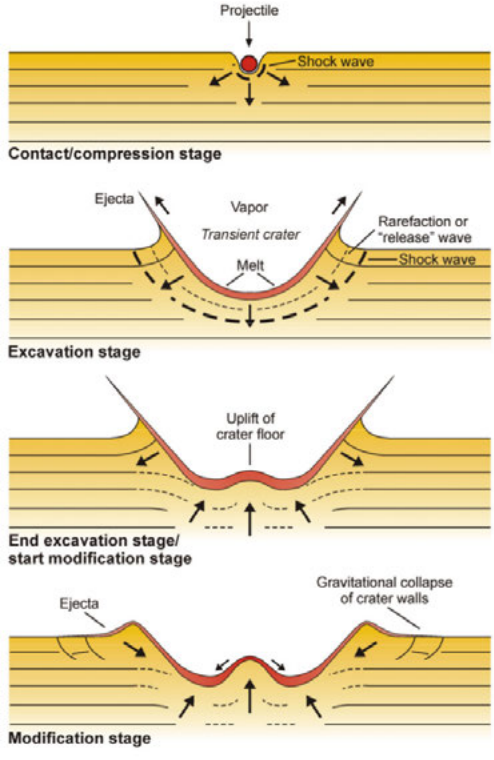

Figure 1.1. Series of schematic cross sections depicting the formation of a terrestrial complex impact structure (i.e., diameter >2–4 km) (Osinski, 2004).

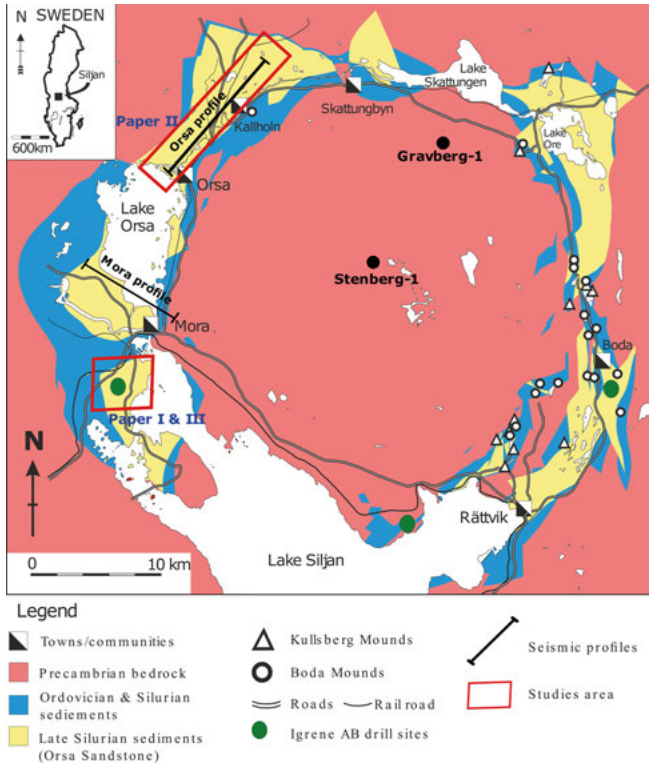

Figure 1.2 Geological map of the Siljan Ring with location of IGRENE AB drill cores sites and the location of seismic profiles marked (modified from Ebbestad and Högström, 2007).

2 Geological background

In this chapter a brief overview of the geological setting in the Siljan Ring impact structure is given. The structure was formed by a meteorite impact, dated as Late Devonian in age (380.9 ± 4.6 Ma, Jourdan et al., 2012). The western side of the Siljan Ring is bordered by the Transcandinavian Granite-Prophyry Belt to the west (1.64-1.74 Ga) and by the Svecofennian Domain to the east (~1.9 Ga) (Collini, 1988). The central uplift part of the structure is ~30 km wide and is composed of Proterozoic magmatic rocks and a mixture of metavolcanic and metasedimentary rocks (with some intrusions) (Fig. 1.2). The Paleozoic rocks are located within the annular ring graben, around the central uplift. Study of the Paleozoic sequences here began in the 19th century, but were often hampered by the lack of outcrops (Wickman, 1981). The Ordovician and Silurian successions deposited in the annular ring graben were preserved from later erosion by the down faulting which occurred during the modification stage of the impact (Kresten et al., 1992). The Obolus beds in the area, belonging to the Early Ordovician, represent the oldest Lower Paleozoic rocks, while the youngest rocks in the area are the Orsa-sandstones (Grahn, 1998). There are several commercial quarries in the Siljan Ring area. These show that the sedimentary rocks are heavily tectonised, generally with sharply inclined or nearly overturned packages of Precambrian rocks and/or sediments.

Several boreholes were drilled in the southern half of the Siljan Ring area by Igrene AB (a small Swedish energy company) for gas exploration down to depths of about 500 m (e.g. Mora 001, Solberga 1 and Stumsnäs 1 in Fig. 1.2). The area around the Siljan Ring was considered to be a stable cratonic region of Baltica before the impact. However, based on core analysis from the Mora 001 and Solberga 1 boreholes (Lehnert et al., 2012) it was deformed by the Caledonian collision prior to the impact. The Mora 001 core study shows a present-day thickness of the Lower Paleozoic rocks to be about 255 m, consisting of a proximately 235 m of Silurian rocks and about 20 m of Ordovician rocks (Lehnert et al., 2012). Within the Silurian succession at about 70 m depth, an approximately 30 m thick sandstone interval is encountered, which is underlain by an approximately 10 m thick siltstone interval (Lehnert et al., 2012). An erosional unconformity is seen between the Middle Ordovician and Early Silurian successions in the Mora 001 borehole where a clear stratigraphic gap is observed. This gap is thought to be due to tectonic loading of thrust sheets and the passing of the forebulge to the west (Lehnert et al., 2012).

In the Mora VM-2 borehole, further to west of the Mora 001 borehole the thickness of the Ordovician limestone changes significantly, where it has a thickness of about 295 m and is overlain by about 95 m of Silurian rocks (Muhamad et al., 2015). The Ordovician successions are more complete in the eastern part of the Siljan Ring than in the western part. In the Stumsnäs 1 core located in southern part of the Siljan Ring, large slabs of Precambrian basement overlying Ordovician limestone rocks were found, which are interpreted to be impact related (Arslan et al., 2013). The maximum total thickness of the Paleozoic rocks in the Siljan Ring is unknown and thought to vary across the structure. A total thickness of Paleozoic strata of 350 m, was estimated in the seismic study by Collini (1988) in the eastern side of the ring. While the Mora seismic profile appears to indicate that the thickness of the Paleozoic is about 600 m (Juhlin et al., 2012).

3 Geophysical methods

The subsurface consists of different types of rocks, which all have different physical properties. Several geophysical techniques have been developed to study these physical properties. The most common of these include seismic, gravity, magnetic and electrical methods, as well as well-logging methods. Regardless of the method, all of them involve data acquisition, processing and, lastly, a data interpretation step. In this chapter I will address the different geophysical methods that I have used in the thesis research.

3.1 Seismic methods

3.1.1 Reflection method

Seismic surveys have been carried out for hydrocarbon exploration since the 1920's (Sheriff and Gerald, 1995). The reflection seismic method is the most widely used geophysical technique available since it provides high resolution images of subsurface structures. This method depends on the contrast between velocity and density of the subsurface horizons. Successful application of seismic methods for hardrock exploration has been documented in a number of studies (e.g., Eaton et al., 2003 and references therein; Malehmir et al., 2012 and references therein). A successful reflection seismic result requires both a well-designed acquisition program and the application of several crucial seismic data processing steps.

3.1.1.1 Seismic data acquisition

In the reflection seismic method, a source is used to generate a seismic wave at the surface that propagates through the subsurface. Seismic receivers placed on the surface then record, among other seismic events, reflections from interfaces with acoustic impedance contrasts. The type of seismic source in use depends on the aim of the study and may include explosives, weight-drop, sledgehammer, air gun or a vibrator. The most common receivers are geophones that measure the ground velocity. Seismic data recording advances year by year to improve data quality and better signal bandwidth. Much of the recent development has led to enhanced efficiency and increased potential for imaging the near surface (e.g., Steeples and Miller, 1998; Reynolds, 2011). To tackle the near surface problems, Uppsala University has recently built a

broadband (0-800 Hz based on digital sensors) multi-component (vertical, transverse and radial components) seismic land streamer system (e.g., Brodic et al., 2015; Malehmir et al., 2015a, 2016 and 2017; Maries et al., 2017) (Fig. 3.1), that can easily be combined with wireless and cabled sensors for various applications (also in Paper III). The system is especially suitable for noisy urban or mining environments or areas where high-resolution images of the subsurface are needed (e.g., Malehmir et al., 2015b). In 2D seismic data acquisition, the source and the receiver points are ideally along a straight line. Straight seismic line geometry generally decreases the ambiguity in seismic data interpretation (Sheriff and Gerald, 1995). Selection of the acquisition geometry is also highly target dependent, particularly if dipping subsurface structures are to be imaged where the seismic line should be perpendicular to the strike of the geological structures (Yilmaz, 2001). The advantages and disadvantages of crooked-line geometries are discussed by Wu (1996) and Nedimovic and West (2003). It is important to have both well-defined goals and knowledge of the area to design a successful seismic survey. This will allow for the proper configuration of the field parameters such as geophone and shot spacing or sample rate etc., which are site and target specific.

Figure 3.1 (a) MEMS-based seismic land streamer developed by Uppsala University towed by a relatively light vehicle. (b) Small cart connecting different segments of the land streamer and also carrying a power unit. (c) The Bobcat-mounted drop hammer drop source owned by Uppsala University (Paper III).

3.1.1.2 Seismic data processing

The data collected by geophones during a seismic survey contain both signal and noise. In the reflection seismic method, we are only interested in the reflected energy. The noise is all the unwanted energy in the data and could be for example coherent noise generated by the seismic source itself, or generated by environmental conditions (wind, rain, snow, human activities, etc.) or ambient noise. The coherent noise is the most troublesome and can be correlated over significant distances and is sometimes aliased with the signal (Ulrych et al., 1999; Özbek, 2000). Therefore, sophisticated processing steps are necessary to enhance the seismic reflection signal and suppress noise. The processing sequence is also related to the geological scenario, data acquisition parameters and the target depth (Yilmaz, 1989). Conventionally, there are three primary stages for seismic data processing; (1) deconvolution, which enhances vertical resolution, (2) stacking, which enhance the S/N ratio, and (3) migration, which enhances the horizontal resolution (Yilmaz, 2001). Additionally, secondary processes may be implemented at different stages to condition the data and enhance the S/N ratio.

Prior to processing, certain preprocessing steps have to be applied. The first step of any preprocessing sequence requires conversion of data from different field formats into SEG-Y format. This is followed by adding the geometry, including coordinates, elevation and shot-receiver configuration. Furthermore, data quality should be checked and most often trace editing is necessary, including deleting dead or noisy traces. When raw seismic data are displayed, it is notable that the amplitude decreases with increasing time on the recorded shot gathers. This is an effect of the geometric divergence related to the waves spreading out spherically from a source, as well as conversion of the seismic energy into heat and other factors such as scattering and transmission losses (Yilmaz, 2001). This amplitude decay requires that amplitude corrections (spherical divergence correction) or amplitude gain control is applied at various stages.

Filtering is also important and is applied through different steps of the reflection seismic data processing sequence. Several types of filtering are used to suppress the noise such as band-pass filtering, dip-filtering and/or time-varying filters. These filters can be designed in the time domain or frequency domain. In general, the filtering process increases the S/N ratio by attenuating low and high frequency noise and outputs an enhanced seismic shot gather that (ideally) contains only the wanted frequencies with no phase change (Khan, 2010). The target of seismic reflection processing is to provide seismic images that represents the correct reflector geometry in the subsurface. However, the surface is often irregular, which means that the source and receiver points along the seismic line don't have the same elevation. Furthermore, near-surface conditions in the weathering layer or loose sediments also vary along the line. This leads to delays or static shifts in travel times of seismic events

that need adjustment. Therefore, static corrections (elevation, refraction and residual statics) are applied to seismic data to compensate for the effect of variation in elevation, weathering thickness, near-surface velocity and to shift the data to a reference datum (Yilmaz, 2001).

Varying source-receiver offsets lead to delays in time for a specific reflection. This appears as a hyperbola in the data, and must be corrected by normal moveout (NMO) corrections. The dip moveout (DMO) correction is applied if dipping layers are present. When the seismic profiles are carried out along a crooked line geometry, the locations of the midpoints (below which reflection points are assumed to be located) are distributed over an area around the actual acquisition line. Here, the cross-dip correction is necessary to correct for potential out of plane events and can significantly improve the coherency of reflected energy and quality of the stacked section (Fig. 3.2) (e.g., Larner et al., 1979; Wu et al., 1995; Nedimovic and West, 2003). The corrected data are then stacked into a (zero-offset) reflection seismic section which significantly improves the S/N ratio. This is followed by the final process of migration. We can define migration as the process that moves the data on the stacked section to its correct position. Migration can be done in both the time or depth domain (Yilmaz, 2001; Kearey et al., 2002). Aside from moving dipping reflectors to their true positions, it also collapses diffractions. The final goal of the migration process is to provide a seismic section comparable to the geological cross section along the seismic line (Yilmaz, 2001). For a more in-depth discussion about seismic data processing, the reader is referred to Yilmaz (2001).

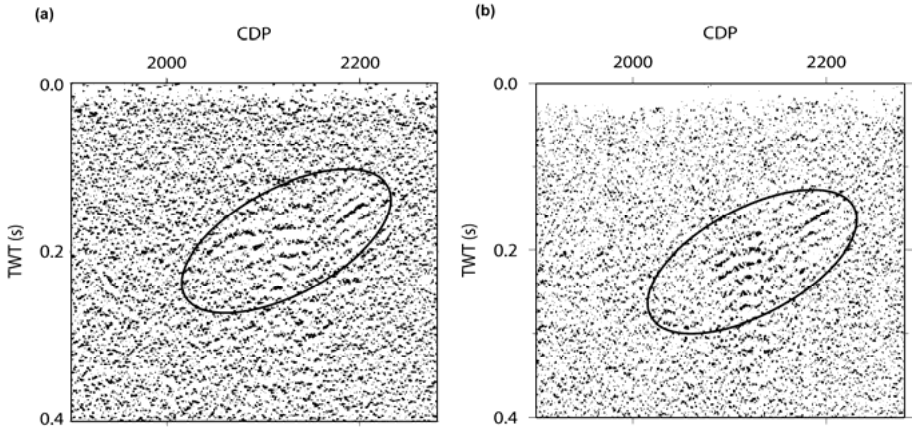

Figure 3.2 A portion of the stacked section along the northern part of the Orsa seismic profile shown (a) without cross-dip correction, and (b) after applying a -15º cross-dip correction (Paper II).

3.1.2 Traveltime tomography

Traveltime tomography is a technique for reconstructing a model of the Earth's seismic velocity using picked first break traveltimes from seismic data. It is a nonlinear problem in the sense that the bending of seismic rays depends on the unknown velocity structure (e.g., Shearer, 1999). Traveltime tomography has a great variety of applications on scales from the near surface (e.g., Zelt et al., 2006) to the deep crust (e.g., Rawlinson and Sambridge, 2003). Reconstruction of the near-surface velocities is especially challenging due to heterogeneities of near surface materials causing changes of the seismic velocity, which in turn increase the nonlinearity of the tomographic inversion. Another important type of tomographic inversion of seismic data focuses on seismic waveform data (e.g., Pratt and Worthington, 1990). In this research, I used first arrival traveltime tomography because it is typically more robust, easier to implement, and computationally less demanding. The purpose of tomographic inversion in this research was to map the velocity structure in the upper few hundred meters along the Orsa seismic profile in order to provide additional information about the formations in the area (Fig. 3.3; Paper II). There are two main steps in traveltime tomography; the forward modeling and the solution of the inverse problem. I have used the PStomo_eq code (Tryggvason et al., 2002) for first break traveltime tomography, in which the forward calculation of traveltimes in the model is a finite-difference approximation of the Eikonal equation of ray tracing (Podvin and Lecomte, 1991; Tryggvason and Bergman, 2006). Once the traveltime field is known for all receivers, the ray paths can be found by reverse ray tracing from the receiver locations perpendicular to the isochrones (Vidale, 1988).

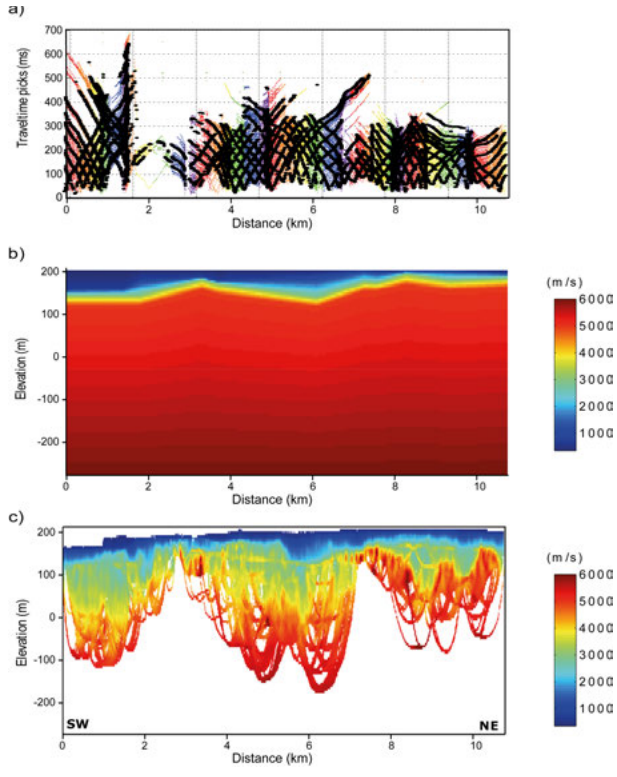

Figure 3.3 Tomography model along Orsa seismic profile (a) First arrival picks, (b) starting model, and (c) final velocity model (Paper II).

3.2 Well logging

The well logging method consists of measuring physical properties of the subsurface rocks. The logging tools are lowered into a borehole in order to measure the physical properties of surrounding rock formations versus depth. Conrad Schlumberger and his brother Marcel Schlumberger introduced and used the first geophysical log in 1927 (Allaud and Martin, 1977). Today there are a number of logging tools that have been developed and used to measure several physical parameters of the rocks. Through borehole measurements it is possible to obtain a vast amount of information which is not necessarily accessible from surface measurements, drill cuttings, and core sampling alone (Key, 1990).

In this section I will describe the logging tools that have been used in this research. These include three different sondes: a temperature sonde (TCD), a three receiver full-waveform sonic velocity sonde (TRSG) and an electrical resistivity sonde. The temperature log (TCD) gives depth-based measurement of fluid temperature and conductivity. It also includes a natural-gamma detector that facilitates more accurate depth correlation with data collected with

other sondes. The sonde is 2.35 m long and has a diameter of 38 mm. The sonic velocity probe is 2.84 m long and has a diameter of 45 mm. The transmitter is located near the bottom of the sonde and the three receivers (RX1, RX2 and RX3) are above it with offsets of 0.86 m, 0.96 m and 1.06 m, respectively. The sonic probe records the travel-time and full-waveform data from an acoustic wave from the transmitter to the three receivers in the probe. A quartz clock in the probe allows high accuracy transit time picking of the first arrivals on the receivers and calculation of the P-wave velocity through rock formations. In addition, it's possible to calculate velocities of the shear and Stoneley waves by further processing the waveform data. The sonic probe also contains a sensor to measure the natural-gamma radiation in the layers, like the TCD mentioned above. The sonic velocity log is usually used with the density log to generate a synthetic seismogram for the purpose of comparison with the seismic data to identify the origin of reflections. The electrical resistivity probe measures the formation resistivity for shallow (single point resistance), medium (16" or short normal) and deep (64" or long normal) penetration depth. Measured potential differences are converted to apparent formation resistivities inside the probe and transmitted digitally to the surface. The probe also measures self-potential (SP), fluid temperature and natural-gamma from the formations around the hole.

3.3 Petrophysical measurements

An important target of geophysical methods is to map the subsurface geology, such as lithological units at depth, thicknesses of formations and structural relationships of the rocks. Therefore, for geophysical data interpretation and for the design of a survey, it is important to have information about the physical characteristics of the rock types (e.g., Birch, 1961). Petrophysical property measurements can be carried out in the field, in boreholes, and in the laboratory using collected samples of outcrops or drill cores. The physical properties of core samples can be used to calibrate and constrain borehole measurements. P- and S-waves velocities can be measured using ultrasonic instruments (Birch, 1961; Jackson et al., 1981; Vanorio et al., 2002; Salisbury et al., 2003; Stanchits et al., 2006; Malehmir et al., 2013; Ahmadi et al., 2013). The ultrasonic instrument used in this research has two transducers that are attached to the rock sample and a pulse/signal generator. One of the transducers is used as a source to transmit the wave signal with a high ultrasonic frequency (e.g., 1 MHz) through the rock sample. The signal is received by the other transducer, which converts it to an electrical signal. The electrical signal is passed to an oscilloscope, which converts it to a digital signal that is displayed by a computer (through additional software). The ultrasonic measurements can be done at room conditions or under pressure (Salisbury et al., 2000; Malehmir

et al., 2013). In my research all measurements were made in room conditions. Uppsala University's ultrasonic lab was used for this purpose.

In addition, we can measure the density of rock samples in the laboratory. The density data can be used with the velocity measurements to generate a synthetic seismogram or/and used in forward modeling of the gravity field. There are various methods to measure the density of a rock sample such as suspension, level and overflow methods (Hughes, 2005). In this research I used the suspension method, which is based on Archimedes' principle. First the dry weight of the sample is measured by an electronic scale. Then the sample is lowered into a water tub to measure the wet weight of the sample. The difference between these two weights divided by the density of the water is used to calculate the sample volume. Then the density of the sample is calculated.

3.4 Gravity method

The gravity method measures the variations in the gravitational field of the earth. Usually the vertical component of the gravitational field is measured at specific locations. The gravity method is based on Newton's law of gravity expressing the force of mutual attraction between two particles in terms of their masses and separation. This law states that two masses *m1* and *m2* with very small dimensions compared to the separation *r* between them will attract each other with a force.

$$F = G(m1.m2)/r^2 \qquad (3.1)$$

Where G is the universal gravitational constant (6.67×10^{-11} $m^3 kg^{-1} s^{-1}$) (Kearey et al., 2002). The gravity method is a passive approach, relatively cheap, reasonably fast in data collection and is usually combined with other geophysical methods (e.g. seismic and magnetic). The gravity method is carried out using a gravimeter, which measures the relative variation of the gravity value between a station and another station as a reference. The gravimeter device needs to be highly sensitive due to the very small variations in density of the subsurface. The common unit of the gravity value is Gal (after Galileo Galilei), which equals one cgs (1 Gal = 1 cm s^{-2}). However, this unit is not convenient for local-scale gravity surveys and usually the measurements are taken in mGal (1 mGal = 10^{-3} Gal). The gravity measurements are affected by several factors and therefore the data should be processed and corrected before the interpretation. These corrections include: (1) the instrument drift correction, (2) the latitude correction, (3) the tide correction, (4) the terrain and elevation correction or free-air correction, and (5) the Bouguer correction. The drift of the instrument can be compensated using a base-station to be reoccupied several times through a day of a survey (repeated measurements). The effect of

the Sun and the Moon on the Earth must be corrected by applying the tidal correction. Gravity readings increase from the equator toward the poles because the shape of the Earth and the rotation. This must be corrected for by the latitude correction. Since gravity decreases as elevation increases it may be necessary to apply a free-air correction. To account for the rock slab between the base station and the measurement station, the gravity effect of it must be compensated for by applying of the Bouguer correction. In addition, a terrain correction is required when measurements are carried out near mountains or valleys. After application of the necessary corrections the so called Bouguer gravity anomaly is obtained, which represents lateral variations of density in the subsurface. The Bouguer gravity map has components of the regional field and the residual (local) field. The regional field is due to large deep structures (or structures outside the area of interest), while the residual field should mainly represent the field due to shallow structures (El-Batroukh and Zentani, 1980; Li and Oldenburg, 1998; Nabighian et al., 2005; Xu et al., 2009; Cella and Fedi, 2012). Depending on the target of the gravity survey, it is usually necessary to separate the residual anomaly from the regional anomaly. There are several sophisticated techniques available for removing the regional anomaly (e.g., Li and Oldenburg, 1998; Malehmir et al., 2007; 2009), the graphical, spectral and low-degree polynomial fitting methods are generally used because of their simplicity (e.g., Nettleton, 1976). The Bouguer anomaly map can be interpreted qualitatively or quantitatively. Furthermore, the gravity data can be modeled in either 2D or 3D. The residual anomaly data are commonly used for the modeling and there are three main types of modeling (1) analytical solutions, (2) forward modeling, and (3) inverse modeling.

3.5 Magnetic method

The magnetic method involves measurements of variations in the Earth's magnetic field and interpretation of the variations. A magnetometer is a device to measure these magnetic variations. A magnetic survey can be made on land, sea or in the air. Magnetic anomalies are due to induced and remanent magnetism. Induced magnetic anomalies are the result of magnetization induced in a body by the Earth's magnetic field. Remanent magnetic anomalies are the result of permanent magnetization of a body. Magnetization is the net effect of all the elemental currents within the magnetic media (Blakely, 1996). The total magnetization of the rocks is equal to the vector sum of induced and remanent magnetizations. The amount of magnetism that rocks are susceptible to having induced is called the magnetic susceptibility. The magnetic susceptibility of rocks are positive values, which implies that the induced magnetic field is parallel to the inducing field. Ground magnetic and aeromagnetic data should be processed before the interpretation. The correction for diurnal variations can be removed by repeat measurements at a base station, which are

made several times through the day of survey. Also the magnetic field of the Earth's core must be subtracted from the total magnetic field data. The International Geomagnetic Reference Field (IGRF) is usually used to remove the effect of the Earth's main field on the survey data. Furthermore, the residual field must be separated from the regional field in a similar manner as for gravity data.

4 Summary of papers

4.1 Paper I: Geophysical borehole data in the Mora area

4.1.1 Summary

The Siljan Ring impact structure is the largest known impact structure in Europe, formed by a Late Devonian meteorite (380.9 ± 4.6 Ma). The central part of the Siljan Ring is uplifted with a diameter of about 20-30 km and outlined by a ring-shaped depression (see Fig. 1.2). The Siljan Ring impact is important for the scientific community and from an economic point of view. Furthermore, the Swedish State Power Board (Vattenfall) conducted several geophysical studies and drilling of shallow boreholes in the area for abiogenic gas exploration in the 1980s (Donofrio et al., 1984; Boden and Eriksson, 1988; Juhlin, 1990; Papasikas and Juhlin, 1997). In addition, Igrene AB (a small Swedish company) drilled several boreholes in the southern half of the Siljan Ring for the purpose of gas exploration. In this paper we report on geophysical down-hole logging data acquired in four boreholes in the Mora area in the southwestern part of the Siljan Ring. The aims of this study were to determine a number of physical properties of the Paleozoic and crystalline rocks in the area. We used three different sondes for the geophysical logging, a temperature sonde (TCD), a three receiver full-waveform sonic velocity sonde (TRSG) and an electrical resistivity sonde (ELTG) (Table 4.1). The temperature sonde measures the fluid temperature (C° unit) and electrical conductivity (μScm unit). The sonde has a sensor to detect the natural-gamma (API unit) activity within the rocks. Clastic rocks such as shale have high natural-gamma activity while limestone or sandstone have low activity. The sonic sonde records full-waveform data on three receivers. We used the first arrival times on the receivers to calculate the P-wave velocity of the formations. This probe also has a natural-gamma sensor. The electrical resistivity sonde records the formation resistivity (Ohm.m unit). The borehole data were processed with depth matching and application of a 25 point median filter before plotting.

In the Mora 001 borehole we ran the temperature and sonic probes to 355.6 m depth (Fig. 4.1). In this borehole we correlated the geophysical logging data with the Mora 001 core lithology that is described in detail by Lehnert et al. (2012). This comparison was used to interpret the log response in the other boreholes. The natural-gamma log of the Mora 001 borehole matches well

with the core lithology after shifting the core lithology column about 5 m upwards (Fig. 4.1). The shale and mudstone show high gamma readings, while the sandstone has low activity within the Silurian succession. The Ordovician limestone shows a low gamma response and has two sharper peaks with high gamma activity in two different depth intervals (Fig. 4.1). These high peaks correlate to high iron ooid concentrations and glauconitic limestones within these depths intervals (see Lehnert et al., 2012 for details). Within the crystalline basement rocks two different response on the gamma log are recorded. One with high gamma reading corresponds to granitic rocks and the other with low gamma reading represents mafic rocks, based on a report by Igrene AB. The first arrival time in the sonic log is picked automatically by the acquisition software and this leads to erratic velocity estimates over some intervals. To improve the velocity calculation we re-picked the first arrival times manually on the three receivers using seismic processing software (Fig. 4.2). The sonic log in the Mora 001 borehole shows a sharp velocity change between the base of the Silurian succession and the underlying Ordovician limestones from about 3000 m/s to about 5500 m/s (Fig. 4.1).

Table 4.1 *Down-hole logging data.*

Boreholes	Depth investigation	Log available
* Mora 001	355 m	TCD (temperature log sonde) TRSG (three receiver sonic sonde)
Vattumyra Production	420 m	TCD (temperature log sonde)
Mora VM 2	94 m	TCD (temperature log sonde) TRSG (three receiver sonic sonde)
Mobillyft	437 m	TCD (temperature log sonde) TRSG (three receiver sonic sonde) ELTG (electric log sonde)

*The core also available.

The Vattumyra Production borehole is close to the Mora 001 borehole (about 6 m separate the two) and was investigated only by the temperature probe to 420 m depth (Fig. 4.3). The natural-gamma log shows a very similar response to the Mora 001 borehole, indicating no changing in lithology and that no major faults exist between these two boreholes. Furthermore, the temperature log in the Vattumyra Production borehole shows an apparent geothermal gradient of about 14 °C km^{-1}, which is less than observed in the Mora 001 borehole.

The Mora VM-2 borehole is located to the southwest of the Mora 001 and Vattumyra boreholes and was investigated with the temperature and sonic sondes to a depth of about 94 m (Fig. 4.4). However, core exists down to a total depth of 508 m (the borehole was deepened in August 2014 to 690 m). The core consists of about 95 m of mudstone and shale, followed by Ordovician limestones to about 390 m depth. The remaining depth interval includes felsic and mafic rocks. The gamma reading shows a similar response to the uppermost 80 m of the Mora 001 and Vattumyra Production boreholes. The

fluid temperature varied between 5.5 and 8 °C, giving an apparent gradient of 25 °C km^{-1}. Also, the velocities are similar to the same depth interval as in the Mora 001 borehole.

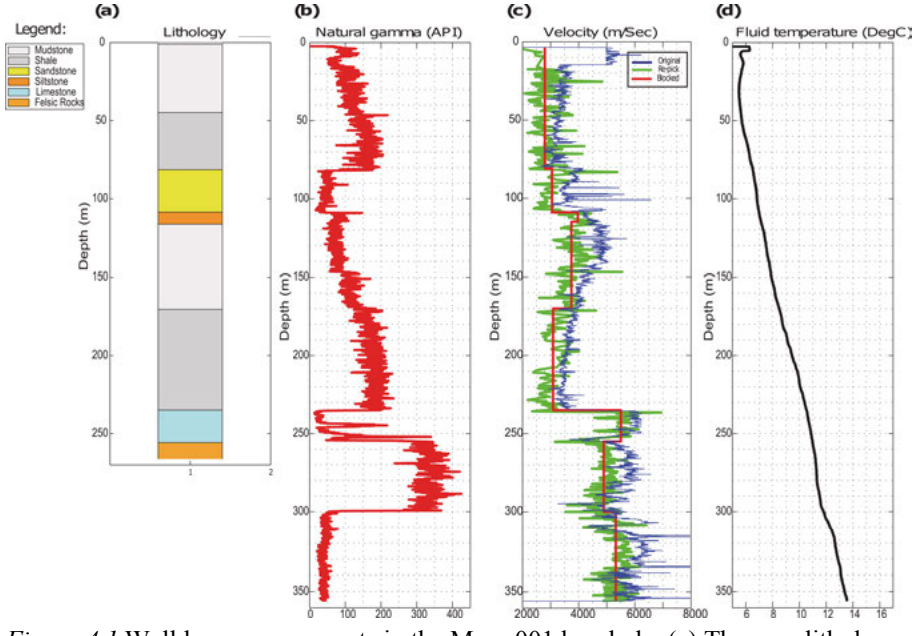

Figure 4.1 Well log measurements in the Mora 001 borehole. (a) The core lithology of the borehole as described by Lehnert et al. (2012). (b) The natural gamma log. (c) The sonic log showing the original, calculated log velocity and blocked velocity. (d) The fluid temperature log.

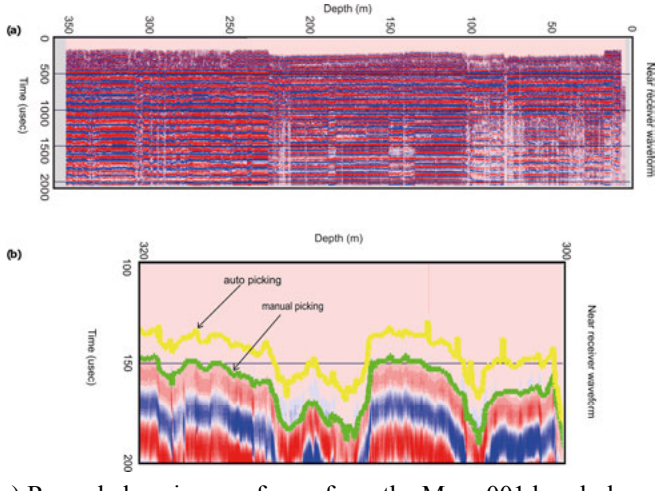

Figure 4.2 (a) Recorded sonic waveforms from the Mora 001 borehole, and (b) automatic and manual picks of first arrivals in the interval 300-320 m.

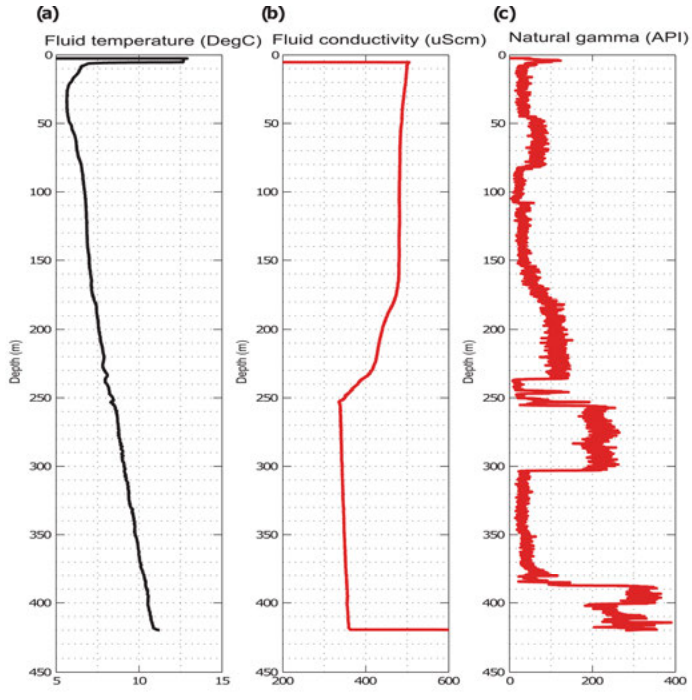

Figure 4.3 Well log measurements at the Vattumyra Production borehole. (a) The fluid temperature log. (b) The fluid conductivity log. (c) The natural gamma log.

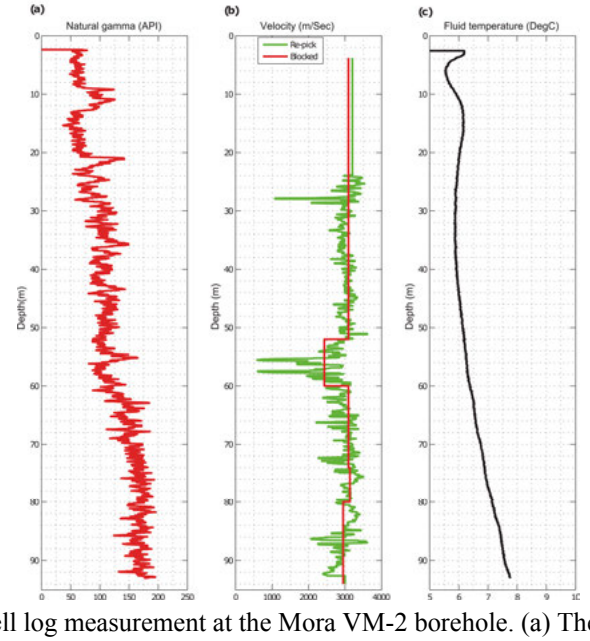

Figure 4.4 Well log measurement at the Mora VM-2 borehole. (a) The natural gamma log. (b) The sonic log showing the calculated log velocity and blocked velocity. (c) The fluid temperature log.

The Mobillyft borehole is located in the northern part of the study area. The temperature, sonic and electrical resistivity probes were run until 437 m depth in this borehole (Fig. 4.5). The geothermal gradient is about 25 °C km^{-1} based on the temperature log and this is similar to that found in the Mora 001 borehole. The natural gamma and sonic log response in the Mobillyft borehole differs in some respects significantly from that of the Mora 001 borehole (Fig 4.6). The upper 140 m consists of shale and mudstone. The following succession correlates well with the core lithology of the Mora MV-3 borehole. The Mora MV-3 core borehole is documented, but not yet logged in detail for its stratigraphy. However, several thrust slice packages and highly radioactive shales are present in the Late Ordovician. The radioactive shales are interpreted to correspond to Fjäcka Shale. These high gamma readings were not observed in the other boreholes. In addition, the sandstone and siltstone layers found in the Mora 001 and Vattumyra Production boreholes are not found in the Mobillyft borehole, indicating that they belong to another tectonic megablock. The resistivity log in the Mobillyft borehole ranges between 1 Ω.m to 12,000 Ω.m before blocking and between 40 Ω.m to 2300 Ω.m after blocking (Fig. 4.5). In general, the resistivity values increase from the top to the bottom of the borehole.

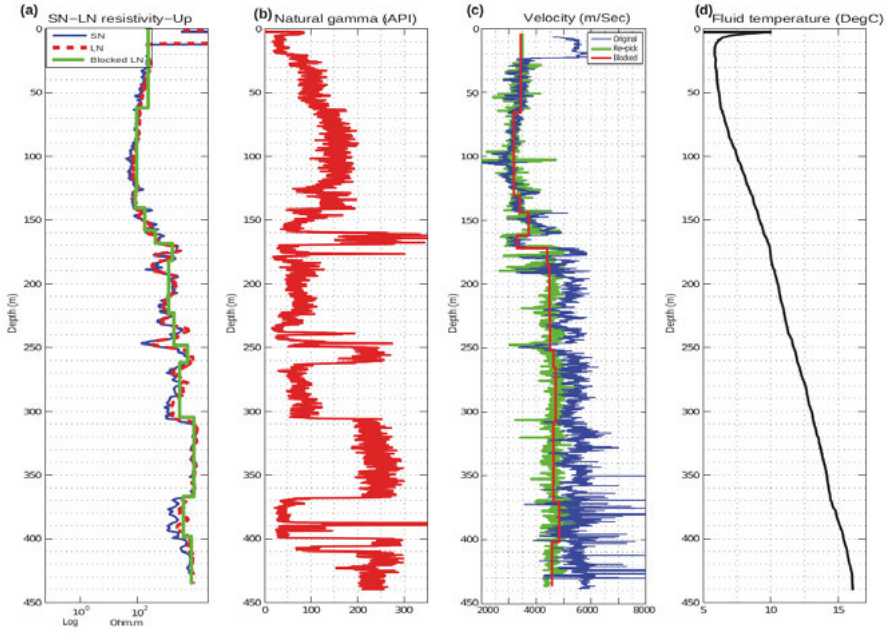

Figure 4.5 Well log measurements at the Mobillyft borehole. (a) The short, long normal resistivity and blocked long normal resistivity. (b) The natural gamma log. (c) The sonic log showing the original, calculated log velocity and blocked velocity. (d) The fluid temperature log.

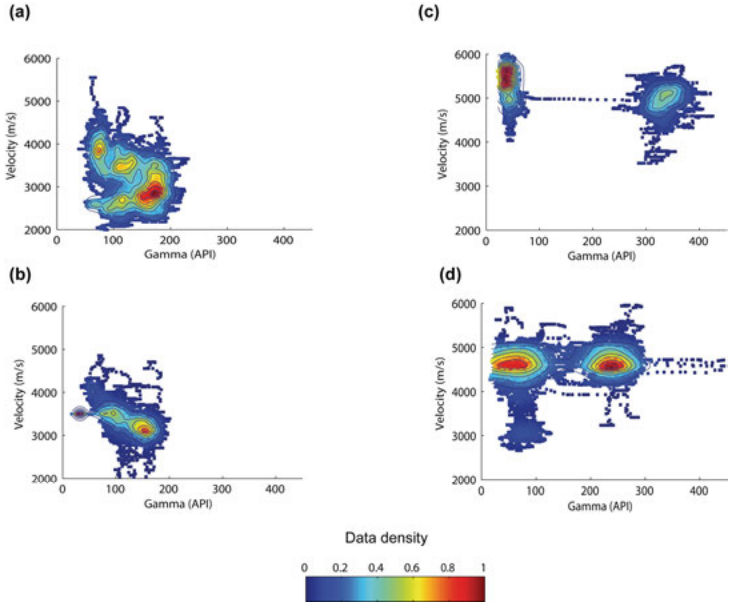

Figure 4.6 Cross-plots of the velocity versus natural gamma (normalized to the maximum) for the shales and mudstones in the (a) Mora 001 and (b) Mobillyft boreholes along with cross-plots of the crystalline rocks for the (c) Mora 001 and (d) Mobillyft boreholes. In the Mora 001 borehole the limestone and sandstone intervals have been removed.

The velocity log from the Mora 001 borehole was blocked based on the gamma log to a limited number of layers. The blocked velocity log and the density measurements from the core samples were used to generate the synthetic seismogram. This seismogram is correlated with the Mora seismic profile, further north of the study area. The synthetic seismogram shows that the boundary between the Silurian and Ordovician successions produces a high amplitude reflection. There is little contrast between the limestones and the underlying granitic rocks. The Mora seismic profile is far from the study area, about 6-7 km to the north. It was interpreted by Juhlin et al. (2012) before there was any borehole velocity data and the interpretation was based on the difference in refracted wave velocities of the layers. The velocities assumed for the interpretation were 3200 m/s for the Silurian succession and about 4000 m/s for the Ordovician limestones. These velocities are low relative to the velocity obtained from the Mora 001 borehole. Therefore, we performed elastic finite-difference seismic modeling (Juhlin, 1995) along part of the profile (Fig. 4.7) with the synthetic data being generated using the values in Table 4.2. However, the velocities in the Ordovician are significantly higher in the logged boreholes than those found from refraction seismic modeling of first arrivals, which are interpreted as propagating through the Ordovician along

the Mora seismic profile. If the velocities of above 4000 m/s on the section of the seismic profile represent lower Silurian mudstones instead, then the Silurian may be up to 450 m thick in this area.

Table 4.2 *Modelling parameters used for Fig. 4.7. HS refers to a half-space.*

	Velocity (m/s)	Model A	Model B	Model C	Model D
Layer 1	600	18	18	18	18
Layer 2	1700	32	32	32	32
Layer 3	3200	204	204	204	204
Layer 4	4050	246	80	124	170
Layer 5	5500	HS	HS	HS	HS

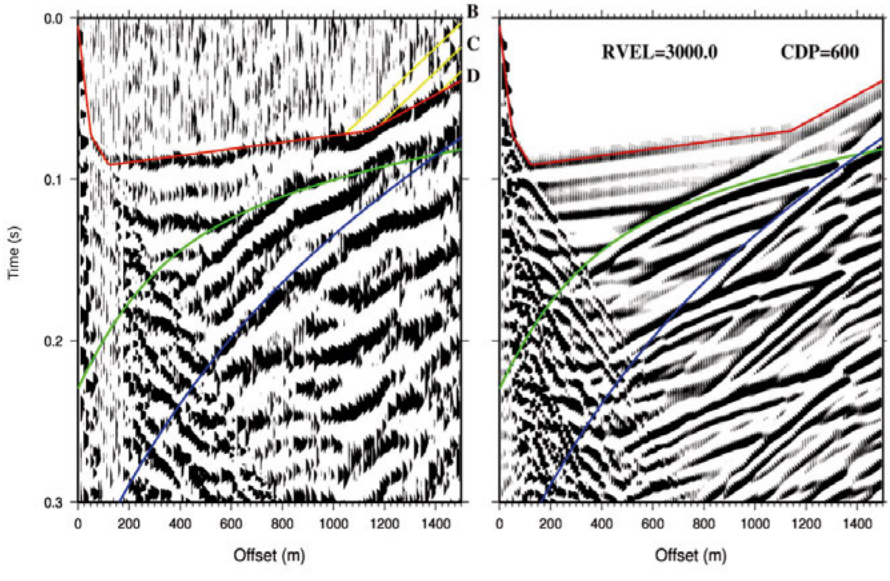

Figure 4.7 (a) A super gather at CDP 600 along the Mora profile. The red line represents the first break times calculated from the velocity-depth Model A in Table 4.2 while the green line represents a reflection from the base of layer 3 in Model A and the blue line a reflection from the base of layer 4 in Model A. The yellow lines are deviations from the first arrival time curve if calculations are made using Models B, C and D. (b) Synthetic gather assuming the velocity structure in Model A. Red, green and blue lines are same as for (a).

Figure 4.8 shows the correlation between the geophysical logs and that the thickness of the Silurian rocks in the Mora 001 and Vattumyra Production boreholes is greater than in the Mora VM-2 and Mobillyft boreholes. In addition, the sandstone and siltstone layers in the Mora 001 and Vattumeyra Production boreholes are absent in the other boreholes. These are due to the presence of different mega-blocks in the area.

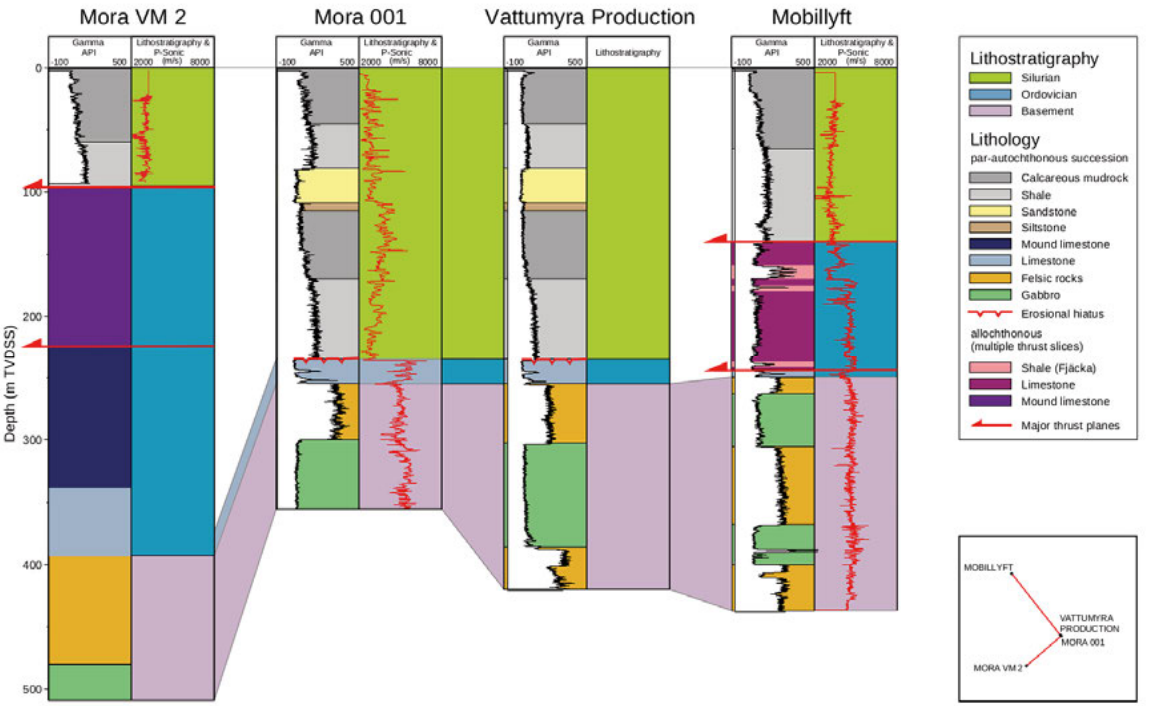

Figure 4.8 Core information from the drill sites together with the geophysical logs in the boreholes show the complexity of the study area. Impact tectonics may explain why cores successions belong to different tectonic megablocks. Lithological interpretation of the logged boreholes takes into account the core lithology of Mora 001 (shown in Fig. 4.1) and the natural gamma logs. The lithology has been grouped into lithostratigraphic units.

4.1.2 Conclusions

Geophysical log data were acquired in the Mora area and compared to the published Mora 001 core, information from the Mora VM-2 and Mora MV-3 cores and the seismic data in the area have highlighted new information on the geological structure and raised new questions. The natural-gamma log response for the Mora 001 and Vattumyra Production boreholes match well with the core lithology and are used as a base for other borehole lithology interpretation. We suggest a complex structure in the study area due to impact related events. The thickness of units and the lithology changes rapidly between wells (Fig. 4.8). In addition, there are several thrust packages in the area making true thickness estimation based only on the geophysical signals impossible. Furthermore, three key horizons with very high gamma reading are observed within the Ordovician limestones.

The velocities observed from the sonic log for the Silurian rocks are consistent with those interpreted as Silurian rocks on the Mora seismic profile. This gives a minimum thickness (about 200 m) of the Silurian along the part of the profile presented in this paper. While the sonic velocities observed in the Ordovician limestones are greater than the velocity of the interpreted Ordovician succession found on the Mora seismic profile. The borehole velocities show a large contrast at the interface between the Silurian and Ordovician successions, which produces a high amplitude reflection on the synthetic seismogram.

The apparent temperature gradient of 23–25 °C km^{-1} in the area is based on the temperature log. This is significantly higher than the 16 °C km^{-1} recorded in the c. 6.5 km deep Gravberg-1 borehole in the northern part of the Siljan Ring (Juhlin, 1991). The high temperature gradient in the study area may be due to the low thermal conductivity of the sedimentary rocks. Thermal modeling is important to study the issue in more detail. Further geophysical work in the area, including seismic surveying and gravity measurements, can help in mapping the complex structures away from the boreholes and discriminating between possible models.

4.2 Paper II: Integrated interpretation of geophysical data in the Orsa area

4.2.1 Summary

The Orsa seismic profile was acquired along a crooked line in 2011 as reported in Juhlin et al. (2012). The profile was 12 km long and located in the northwestern part of the Siljan Ring (Fig. 1.2). In addition, four seismic lines were acquired in the study area by Oljeprospektering AB (OPAB) in 1979. These seismic data were only available as scanned tiff images of the final stacked sections. However, these images were converted to SEGY format using a MATLAB script (Sopher, 2016). The data acquisition parameters of the OPAB seismic data and Orsa seismic profile are given in Tables 4.3 and 4.4, respectively.

Table 4.3 *Acquisition parameters for the OPAB data.*

Parameters	Value
Recorded by	Seismic Geocode Ltd.
Seismic source	Mini sonic
Source characteristics	2 Rammers
Source depth	Surface source
Source interval	30 m
Offset from first channel	45 m
Number of geophone stations	12
Geophone interval	30 m
Geophone type	Sensor SM-4 30 Hz
Spread type	In line
Record length	0.5 s
Sample interval	1 ms
Low cut filter	80 Hz slope of 24 dB/Oct
High cut filter	None
Date	July 1979

In this study, we reprocessed the Orsa seismic profile in an attempt to better map the thicknesses of the sedimentary rocks along it. This reprocessing along with first break traveltime tomography, vintage seismic profiles from the 1970s (OPAB data), new and pre-existing gravity data, aeromagnetic data and the bedrock geology information are used to constrain the nature of the Paleozoic structure and uppermost crystalline rocks. The processing workflow applied to the data in this study is listed in Table 4.5. A number of additional processing steps were applied, relative to the original processing of the data. These include a cross-dip correction of -15^{o}, which was applied to improve the image from the seismic data (Fig. 3.2) and a dip moveout (DMO) correction. Additional velocity analysis was also performed. In the reprocessing we improved the final seismic stacked and migrated sections compared to the previous processing (Figs. 4.9 and 4.10). The new sections show more distinct

and continuous reflections in the uppermost 300 ms. Furthermore, we converted the migrated section to a depth section. The northern part of the profile is more reflective than the southern part of the profile. There are no deeper boreholes in the area to provide information about the origin of the reflections on the Orsa seismic section.

Table 4.4 *Data acquisition parameters for the Orsa seismic profile.*

Acquisition geometry	Split spread
Number of channels	320 (160-160)
Near offset	0 m
Geophone spacing	10 m
Geophone type	28 Hz single
Source spacing	20 m
Source type	VIBSIST 3000
Hit interval between hammer blows	100- 200 ms
Sweeps per source point	3-4
Nominal fold	80
Recording instrument	SERCEL 428UL
Sample rate	1 ms
Field low cut	Out
Field high cut	400 Hz
Record length	30 s
Profile length	12 km
Source points	542
Dates acquired	10/06/-15/06,2011

On the OPAB profiles there appears to be two reflective horizons. The shallow reflection can be correlated across the majority of the sections (Fig. 4.11). We interpreted the shallow reflection to represent the top of the Ordovician, while the deeper reflection to represent the top of crystalline basement. The Ordovician succession appears to have a relatively constant thickness on the OPAB lines in places where both reflections are present. Based on the new processing and OPAB profiles we adjusted the previous interpretation of the Orsa profile presented by Juhlin et al. (2012) (Fig. 4.12). In this new interpretation, we interpreted the Ordovician rocks along the Orsa profile to have a constant thickness about 200 m and the Silurian succession is interpreted to have a thickness up to about 400 m (Fig. 4.12). The sub-horizontal reflection within the crystalline basement at about 2.5 km has been interpreted to be from a dolerite sill (Juhlin et al., 2012).

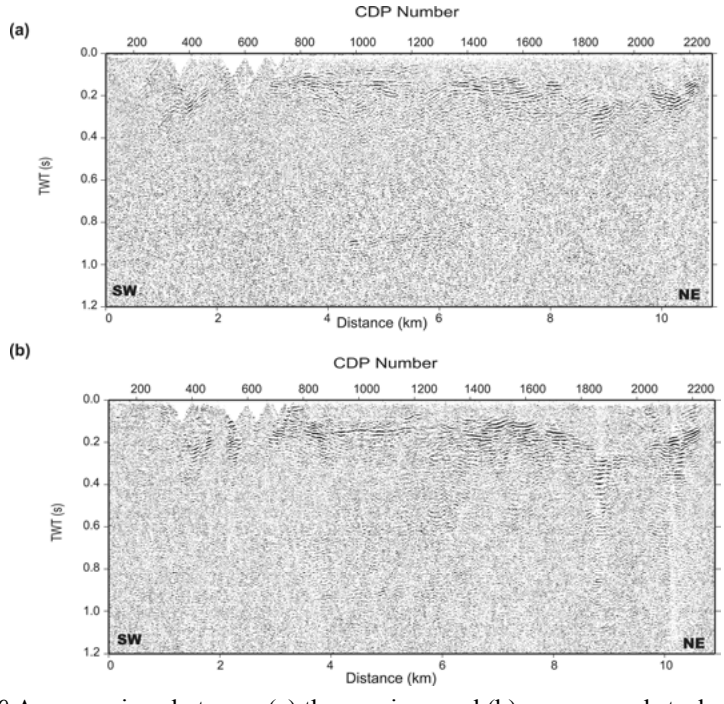

Figure 4.9 A comparison between (a) the previous and (b) reprocessed stacks of the Orsa seismic data.

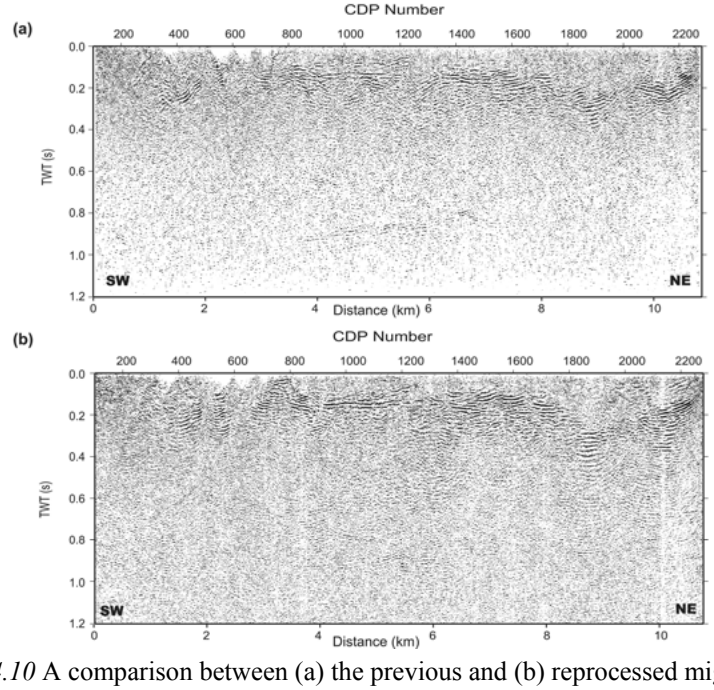

Figure 4.10 A comparison between (a) the previous and (b) reprocessed migrated Orsa seismic section.

Table 4.5 *Data processing applied to the Orsa seismic profile in this study.*

Step	Parameters
1	Read decoded VIBSIST data
2	Bulk static shift to zero time
3	Apply geometry
4	Pick first breaks
5	Spherical divergence correction
6	Trace editing
7	Trance balance: 0-3000 ms
8	Spectral equalization: 0-600 ms: 50-80-200-240 Hz 700-1500 ms: 40-70-180-240
9	Time variant bandpass filter: 0-400 ms: 50-80-240-360 Hz 450-600 ms: 45-70-210-300 Hz 700-1000 ms: 40-60-180-270 Hz 1100-3000 ms: 35-50-150-225 Hz
10	Refraction statics: datum 180 m, replacement velocity 3000 m/s
11	Cross-dip correction (-15^{o})
12	Residual statics
13	Median filter: 11 traces, 3 samples,1600,2000,2400 m/s, subtract
14	AGC: 50 ms
15	Residual statics
16	Velocity analysis
17	NMO correction: 70% stretch mute
18	DMO correction
19	Trace balance
20	FX Decon: 19 trace window
21	Dip filter 1.5 ms/trace cutoff
22	Trace balance
23	Stolt migration: 200-3000, 1000-4000 ms/s
24	Time-depth migration

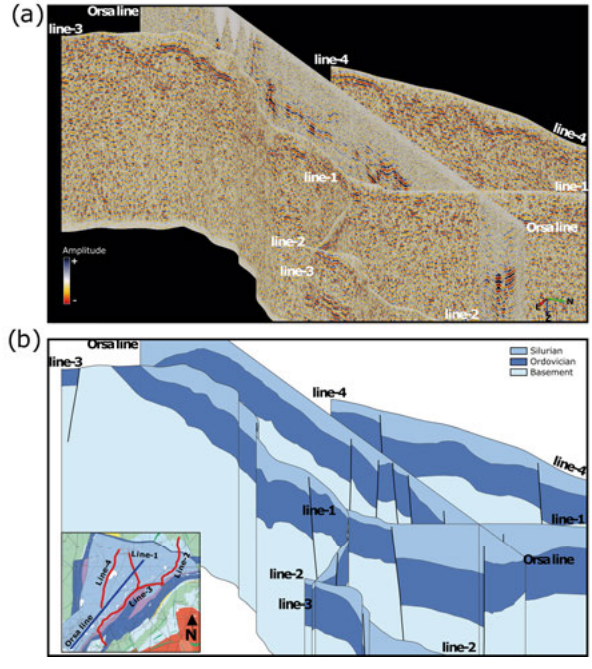

Figure 4.11 (a) 3D visualization of the unmigrated seismic sections (Orsa profile and OPAB sections), (b) Interpretation of the seismic sections.

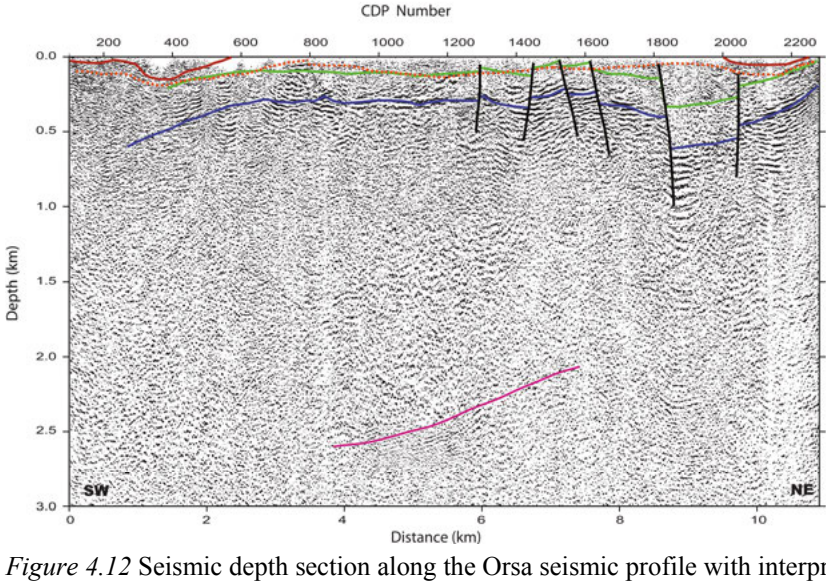

Figure 4.12 Seismic depth section along the Orsa seismic profile with interpretations of the geological boundaries. Brown line corresponds to the base of the water saturated loose sediments, orange dotted line to the base of the Silurian as interpreted from the refraction velocities in Juhlin et al. (2012), green line to the base of the Silurian assuming the Ordovician to have a relatively constant thickness, blue line to the base of the Ordovician, pink line to a dolerite intrusion, black lines to faults.

Traveltime tomography was performed in 3D using the PStomo-eq algorithm (Tryggvason et al., 2002). A total of 538 shots with 90,918 first break picks were used for the tomography. Furthermore, we used a 2D starting model after testing a number of 1D models. The final velocity model (Fig. 3.3) was obtained after 9 iterations with an RMS of 2.8 ms and includes velocities ranging from between 800 m/s to 6000 m/s. A total of 69 ground gravity points were measured along the Orsa seismic profile in this study and merged with gravity point data provided by SGU. These data were then processed by applying standard data reduction methods using a density 2.67 g/cm^3. After that, we separated the regional field from the Bouguer anomaly map using a 2nd order quadratic polynomial and then subtracted this from the Bouguer anomaly map to obtain the residual map (Fig. 4.13). Based on the geological map of the study area the gravity highs represent basic and intermediate volcanic rocks, while the low gravity values indicate sedimentary and felsic intrusive rocks. The aeromagnetic data (Fig. 4.14) were provided by SGU and we followed a similar workflow to separate the regional field as for the gravity data (Fig. 4.14). Total-field magnetic intensity, inclination and declination used were 50,634 nT, 73.1° and 4.5°, respectively (www.geomag.nrcan.gc.ca). Remnant magnetization was ignored since there are no petrophysical samples available to us from the study area.

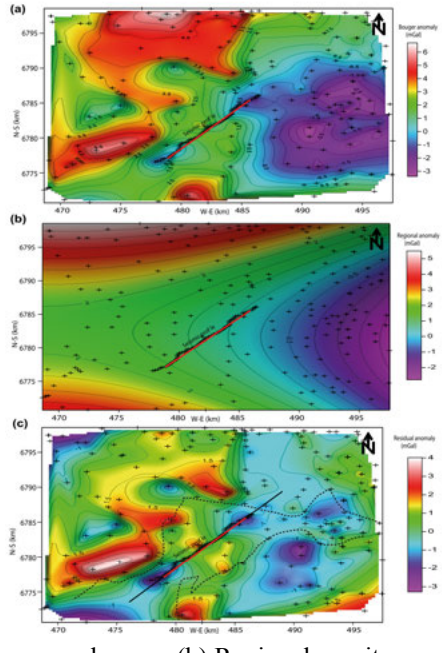

Figure 4.13 (a) Gravity anomaly map, (b) Regional gravity anomaly map and (c) Residual gravity anomaly map of the study area with the outline of the limits of the Paleozoic rocks marked by the thick black line. Plus (+) symbols represent the gravity ground stations. The red line shows the location of the Orsa seismic line, while the thin black line shows the profile used for the gravity modeling.

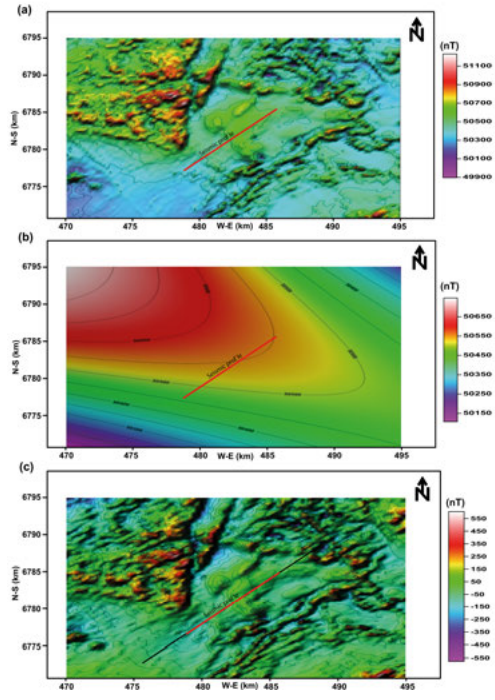

Figure 4.14 (a) Aeromagnetic anomaly map, (b) Regional magnetic anomaly map and (c) Residual magnetic anomaly map of the study area. The red line shows the location of the Orsa seismic line, while the thin black line shows the profile used for the magnetic modeling.

We used the residual of gravity and aeromagnetic data along the Orsa profile to perform 2.5D forward modeling using the ModelVison^{TM} software. A background with zero density contrast and susceptibility was used for the modeling. The interpretations outlined from the migrated and depth sections were used as a basis for the initial geological model due to the lack outcrops or drilled boreholes in the study area. Three layers were used to represent the subsurface geology with different density and susceptibility contrasts to fit the model with the obtained data (Fig. 4.15). The upper layer representing Quaternary sediments and the middle one Paleozoic rocks had density contrasts of -0.62 g/cm^3 and -0.1 g/cm^3, respectively. The lower layer, representing the crystalline basement, was assigned a density contrast of +0.023 g/cm^3. In order to fit the gravity data we had to introduce two rectangular bodies with a high density contrast, +0.1 g/cm^3, (Fig. 4.15). These two bodies are located in the area where the assumed basement seismic reflection appears to be strongest, which is consistent with the inferred presence of more mafic rocks. The density model matches the obtained data better than the magnetic model. This may be related to the constant parameter values assigned to the layers in the model.

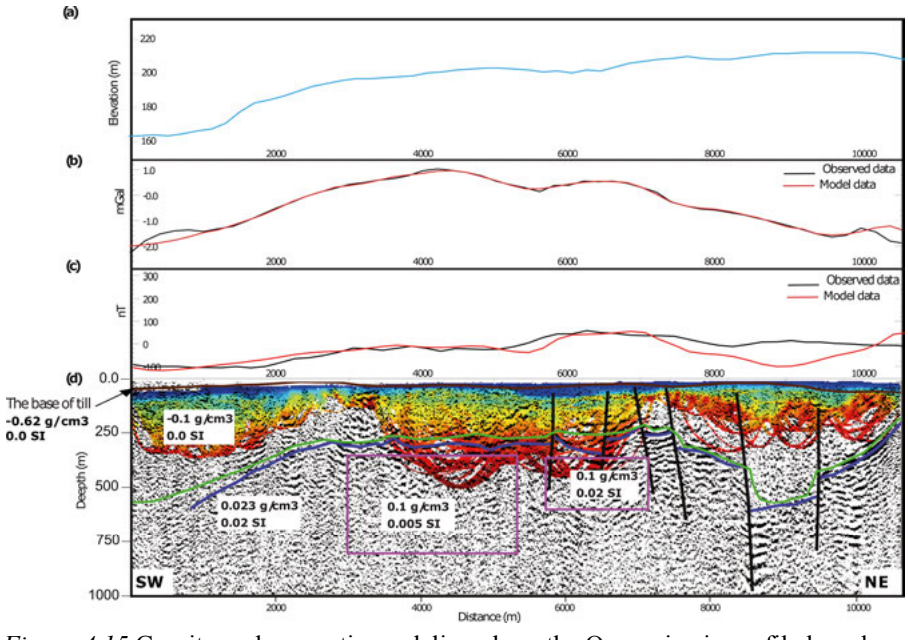

Figure 4.15 Gravity and magnetic modeling along the Orsa seismic profile based on the interpretation of the seismic reflection data. (a) Topographic profile. (b) Gravity model. (c) Magnetic model. (d) Integration of the seismic section, tomography and model based on the interpretation of the potential field data. The blue line represents the boundary between the sedimentary rocks and the basement and the thin black lines indicate faults. The brown line is the base of the loose sediments and the green line represents the boundary between the sedimentary rocks and the basement based on the potential field data modeling. The pink boxes represent two high density bodies within the crystalline basement. The numbers in white boxes in (d) represents the density and susceptibility contrast.

4.2.2 Conclusions

We used the reprocessed Orsa seismic profile with first break traveltime tomography, vintage seismic OPAB profiles, new and pre-existing gravity data, aeromagnetic data and the bedrock geological map to present a geological model along the profile. The reprocessing, most importantly the cross-dip correction step, improved the final stacked and migrated sections compared to the original processing. Using the reprocessed profile and the interpreted OPAB data a simple geological model consistent with the surface geological map was constructed. There are two relatively clear reflection horizons in the seismic data, where the upper reflection is interpreted to be the top of the Ordovician and the lower one to be the top of the basement. The traveltime tomography results are generally consistent with the model, except in the northern part of the Orsa profile where high velocity material is found in the interpreted Silurian succession. The 2.5D gravity forward modeling corresponds better to the

observed data obtained than the magnetic modeling. Scientific drilling is required in the area to verify our interpretation.

4.3 Paper III: High-resolution 2D seismic reflection investigations in the Mora area

4.3.1 Summary

In this study we focus on the southwestern part of the impact, as in paper I, with the main objective to map the Paleozoic successions and structure and to determine what faults might be present in the Mora area. During the summer of 2015 four seismic lines were acquired in the Mora area within 5 days with a total length of about 3 km (Fig. 4.16). For the data acquisition we used the 3C MEMs-based land streamer system of Uppsala University combined with wireless recorders (Brodic et al., 2015). The system was designed for noisy environments and high-resolution imaging of the subsurface. We used a Bobcat drop hammer as a seismic source (Fig. 3.1). The shot spacing was 4 m and to increase the signal to noise ratio we recorded 5 hits at each shot position. A summary of the main acquisition parameters is shown in Table 4.6. Processing of the seismic data was performed to attenuate the noise and enhance the reflections. Table 4.7 shows the main processing steps applied to the data. We used only the vertical component of the land streamer data combined with the 1C wireless data. Data quality varied along the lines depending upon the near surface conditions, traffic influence and industrial noise. The stacked data along the profiles were migrated using a finite-difference algorithm. Thereafter the sections were converted to approximate depth sections by using an appropriate interval velocity for each line.

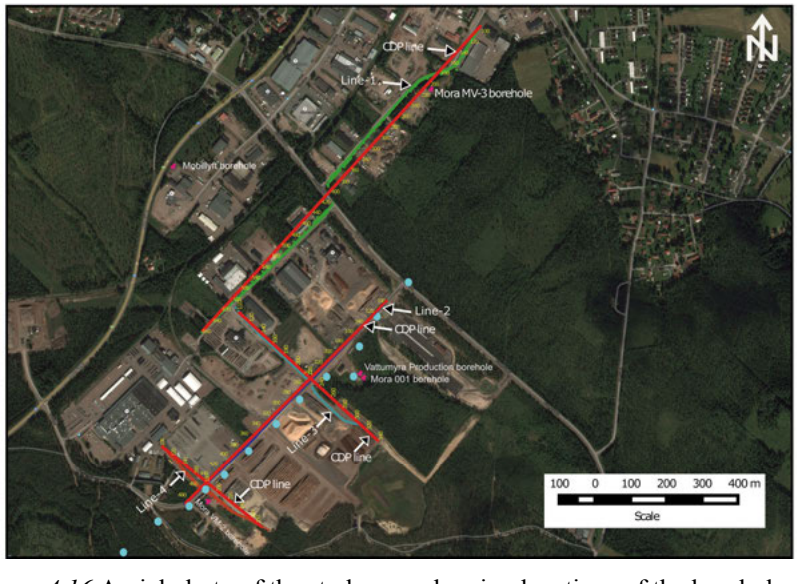

Figure 4.16 Aerial photo of the study area showing locations of the boreholes (pink symbols), ground gravity points (cyan circles) and the reflection seismic lines (red lines, yellow numbers indicate CDP number).

The lithology of the wells in the area show significant changes between boreholes (Muhamad et al., 2015). In the Mora 001 core approximately 235 m of Silurian rocks are present, underlain by a thin section of Ordovician limestones (Lehnert et al., 2012). Unlike the other wells in the area, the Mora 001 core appears to represent a sequence largely unaffected by faulting and impact related deformation, hence it is considered here to be representative of the pre-impact sequence. In the Mora VM-2 core the Silurian rock thickness is about 95 m and with a similar lithology to the upper part of the Mora 001 core. However, the Ordovician limestones are approximately 300 m thick, in stark contrast to observations in the Mora 001 core. Several thrust faults are observed to intersect the Mora VM-2 core, most notably, faults can be identified between the Ordovician and Silurian sections in the well and also within the thick Ordovician succession (Muhamad et al. 2015). The Mora MV-3 borehole is located on Line 1 (Fig. 4.16). Preliminary inspection of the core data (based mainly on Igrene AB images of core boxes) demonstrate in this study that the sequence is highly deformed, where the thick Ordovician-Silurian sequence is primarily due to the development of a thick package of thrust slices which lead to repetition of the sequence. The contrast in the thickness of the Silurian and Ordovician successions between these wells and the presence of a large number of faults highlights the variability and complexity of the sedimentary sequence in this area.

Table 4.6 *Data acquisition parameters.*

Parameters	Line 1	Line 2	Line 3	Line 4
Recording system	SERCEL 428	SERCEL 428	SERCEL 428	SERCEL 428
Source type	Bobcat drop hammer	Bobcat drop hammer	Bobcat drop hammer	Bobcat drop hammer
Sweeps	5 hits	5 hits	5 hits	5 hits
Sample rate(ms)	1	1	1	1
Recording length (s)	25 (1 used)	25 (1 used)	25 (1 used)	25 (1 used)
Sensors	DSU3, Streamer, 1C Wireless	DSU3, Streamer, 1C Wireless	DSU3, Streamer, 1C Wireless	DSU3, Streamer, 1C Wireless
Receiver spacing (m)	2-4 (streamer), 4-20 (wireless)	2-4 (streamer), 4-20 (wireless)	2-4 (streamer), 4-12 (wireless)	2-4 (streamer), 12 (wireless)
Shot spacing (m)	4	4	4	4
Number of receivers	80 landstreamer, 47-1C wireless	80 landstreamer, 47-1C wireless	80 landstreamer, 50-1C wireless	80 landstreamer, 33-1C wireless
Number of shots	388	185	152	92
Profile length (m)	1150	790	540	350

Table 4.7 *Processing steps and parameters.*

Line 1	Line 2	Line 3	Line 4
Read SEGD data	Read SEGD data	Read SEGD data	Read SEGD data
Extraction of vertical component	Extraction of vertical component	Extraction of vertical component	Extraction of vertical component
Stacking of weight-drop gathers	Stacking of weight-drop gathers	Stacking of weight-drop gathers	Stacking of weight-drop gathers
Apply geometry (CDP bin size 2 m)	Apply geometry (CDP bin size 2 m)	Apply geometry (CDP bin size 2 m)	Apply geometry (CDP bin size 2 m)
Pick first breaks	Pick first breaks	Pick first breaks	Pick first breaks
Spherical divergence correction	Spherical divergence correction	Spherical divergence correction	Spherical divergence correction
Trace editing	Trace editing	Trace editing	Trace editing
Trace balance	Trace balance	Trace balance	Trace balance
Spectral equalization:	Spectral equalization:	Spectral equalization:	Spectral equalization:
50-80-200-240 Hz	50-80-200-240 Hz	50-80-200-240 Hz	80-100-200-250 Hz
Wiener deconvolution	Wiener deconvolution	Wiener deconvolution	Wiener deconvolution
Band pass filter:	Band pass filter:	Band pass filter:	Band pass filter:
0-200 ms: 30 70 150 250 Hz	0-200 ms: 30 70 150 250 Hz	0-200 ms: 30 70 150 250 Hz	70-100-200-250 Hz
300-600 ms: 25-60-120-240 Hz	300-600 ms: 25-60-120-240 Hz	300-600 ms: 25-60-120-240 Hz	Refraction static : datum 193 m,
650-1000 ms: 15-40-100-220 Hz	650-1000 ms: 15-40-100-220 Hz	650-1000 ms: 15-40-100-220 Hz	replacement velocity 3000 m/s
Refraction static : datum 195 m,	Refraction static : datum 195 m,	Refraction static : datum 193 m,	AGC : 50 ms
replacement velocity 3000 m/s	replacement velocity 3000 m/s	replacement velocity 3000 m/s	Median filter: 13 traces, 2000 m/s, subtract
AGC : 50 ms	AGC : 50 ms	Mute	Mute
Mute	Mute	Residual static	Velocity analysis
Residual static	Residual static	AGC : 50 ms	NMO correction: 70% stretch mute
Velocity analysis	Velocity analysis	Velocity analysis	Stack
NMO correction: 70% stretch mute	NMO correction: 70% stretch mute	NMO correction: 70% stretch mute	Migration: finite difference
DMO correction	Stack	Stack	Zeromute
Stack	Trace balance	Trace balance	Time-to-depth conversion
Trace balance	Dip filter 1.7 ms/trace cutoff	FX Decon: 19 trace window	
FX Decon: 19 trace window	Trace balance	Trace balance	
Dip filter 1.5 ms/trace cutoff	Migration: finite difference	Migration: finite difference	
Trace balance	Zeromute	Zeromute	
Zeromute	Time-to-depth conversion	Time-to-depth conversion	
Migration: finite difference			
Band pass filter : 20-40-150-250 Hz			
Zeromute			
Time-to-depth conversion			

The core boxes of the Mora VM-2 borehole were available and 42 samples were taken from different lithologies, spread throughout the entire core, for the purpose of petrophysical data measurements (Table 4.8). In order to compare the Mora VM-2 borehole lithology with the seismic data from Line 2 and Line 4 a synthetic seismogram was generated. Since no geophysical sonic and density logs were available for the Mora VM-2 borehole we used the P-wave velocity and density measurements from the core samples to generate blocked pseudo velocity and density logs, then we generated the synthetic seismogram (Fig. 4.17). The boundary between the Silurian and Ordovician rocks produces a high amplitude reflection in the synthetic seismogram.

In addition, 13 ground gravity points were acquired in 2013 along Line 2 (Fig. 4.16). The data were processed to calculate the Bouguer anomaly and

then used together with additional gravity data provided by the Geological Survey of Sweden (SGU) in the study area to generate the Bouguer anomaly map (Fig. 4.18). After that the residual anomaly map, which generally represent shallow subsurface structures, was sepa-rated from the regional anomaly map in the area (Fig. 4.18).

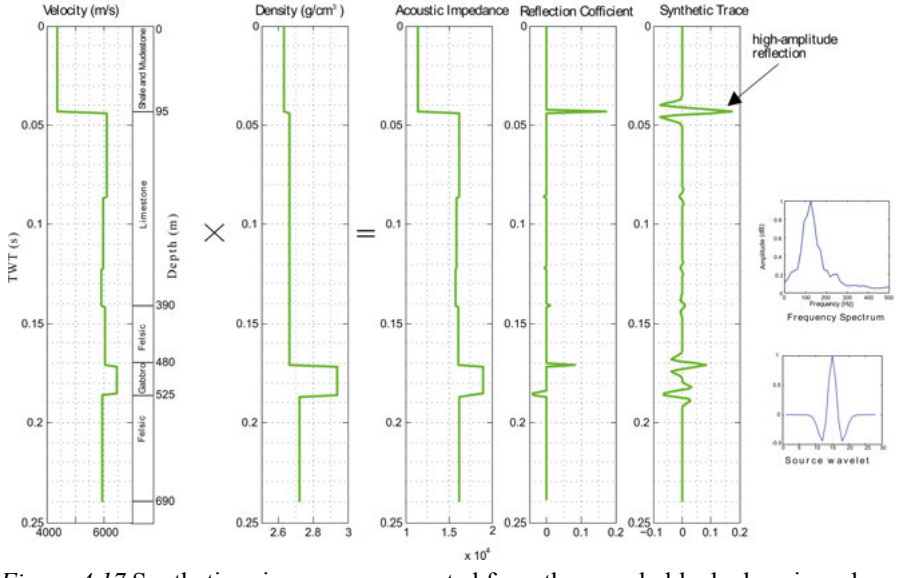

Figure 4.17 Synthetic seismogram generated from the pseudo blocked sonic and density logs in the Mora VM-2 borehole.

The results of seismic data processing show a number of clear seismic reflections (Figs. 4.19 - 4.22). The quality of the seismic images also varies along the seismic lines, which is likely due to changes in near surface conditions, environmental noise and the maximum offset between the source and receiver. Therefore, despite the availability of well data, the interpretation of the data is still highly subjective. Line 1 (Fig. 4.19) is the longest line and more reflections are present than on the other seismic lines. The sedimentary rocks are more reflective than the basement rocks along this line. The interpretation and identification of the origin of reflections is difficult due to the tectonised nature of the lithology in the northeast, as based on the Mora MV-3 core log study. It is likely that the seismic reflections, which are abundant in this part of the section, are not representative of the original bedding of the sequences, but instead are related to lithological contrasts along the fault planes of the thrust slices.

Table 4.8 *Petrophysical data measurements on core samples from the Mora VM-2 borehole.*

Lithology	Depth (m)	No. of samples	Average p-wave velocity (m/s)	Average density (g/cm^3)
Shale and Mudstone	0–95	6	4361	2.63
Limestone	95–225	7	6104	2.64
Limestone	225–335	9	5990	2.67
Limestone	335–390	6	5930	2.69
Felsic rocks	390–480	4	6045	2.64
Mafic rocks	480–525	4	6455	2.94
Felsic rocks	525–690	6	5953	2.69

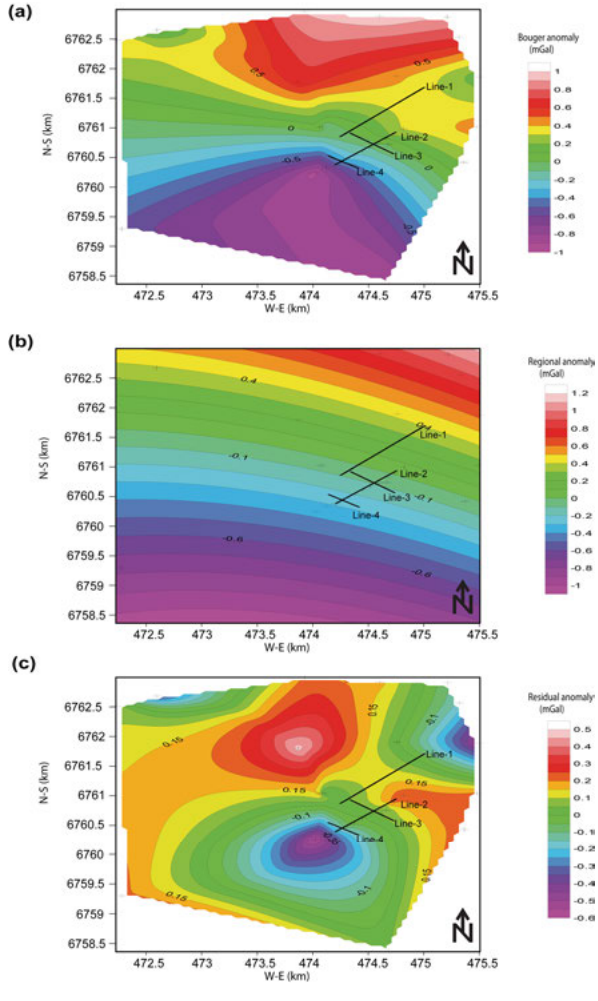

Figure 4.18 (a) Gravity anomaly map, (b) Regional gravity anomaly map and (c) Residual gravity anomaly map of the study area. Plus (+) symbols represent the gravity ground stations. The black lines shows the locations of CDPs seismic lines.

The depth converted seismic section and interpretation of Line 2 is shown in Figure 4.20. The northeastern part of the line is more reflective than the southwestern part. There are two core boreholes (Mora 001 and Mora VM-2) located on this line (Fig. 4.16) that were used for comparison. The reflective northeastern half appears to correspond to the basement and top Ordovician interfaces based on the data from the Mora 001 well. We interpreted a fault plane to be present to the southwest of the Mora 001 well, which separates an undisturbed block in the northeastern part from a disturbed block in the southwest (Fig. 4.20). The gravity data along this line was used to check for consistency with the seismic interpretation along it. The residual anomaly map was used as a basis for 2.5D forward density modeling along Line 2. In addition, the density measurements from the Mora VM-2 core samples (Table 4.8), the lithology of the boreholes (Mora 001, Vattumyra Production and Mora VM-2 boreholes) and the interpretation outlined along seismic Line 2 were used to construct the forward model of the subsurface geology (Fig. 4.23). The gravity anomaly increases from southwest to northeast along the profile and the best fit between the density model response and the measured data was obtained using the layer density contrasts shown in Table 4.9.

Table 4.9 *Density contrast used for gravity modeling along Line 2.*

Layer	Density contrast (g/cm^3)
Sediments	-0.67
Paleozoic rocks	-0.01
Basement rocks	0.086

Figure 4.21 shows the depth converted seismic data and interpretation for Line 3. No well data are available on this line to help constrain the interpretation. Based on the intersection with Line 2, we suggest that the NW part of the profile is part of the relatively undeformed fault block which the Mora 001 well intersects. We interpret a large fault to be present on this line at CDP 240. As on Line 2, we observe normal displacement at the basement level, but indications of compression in the shallower reflections to the SE of the fault plane. The large fault on Lines 2 and 3 is one of the features on the seismic data which can be interpreted with a higher degree of confidence. This fault appears to be a normal fault which was later inverted, implying a period of extension followed by compression.

The depth converted seismic section for Line 4 is shown in Figure 4.22. This line is the shortest line and has the weakest seismic response of the four lines in the study area. It isn't possible to make a confident interpretation along this line, since we have only one clear reflection in the center of the line. The poor seismic response along this line could be due to a combination of highly complex subsurface structure, suboptimal seismic acquisition parameters and poor near surface conditions.

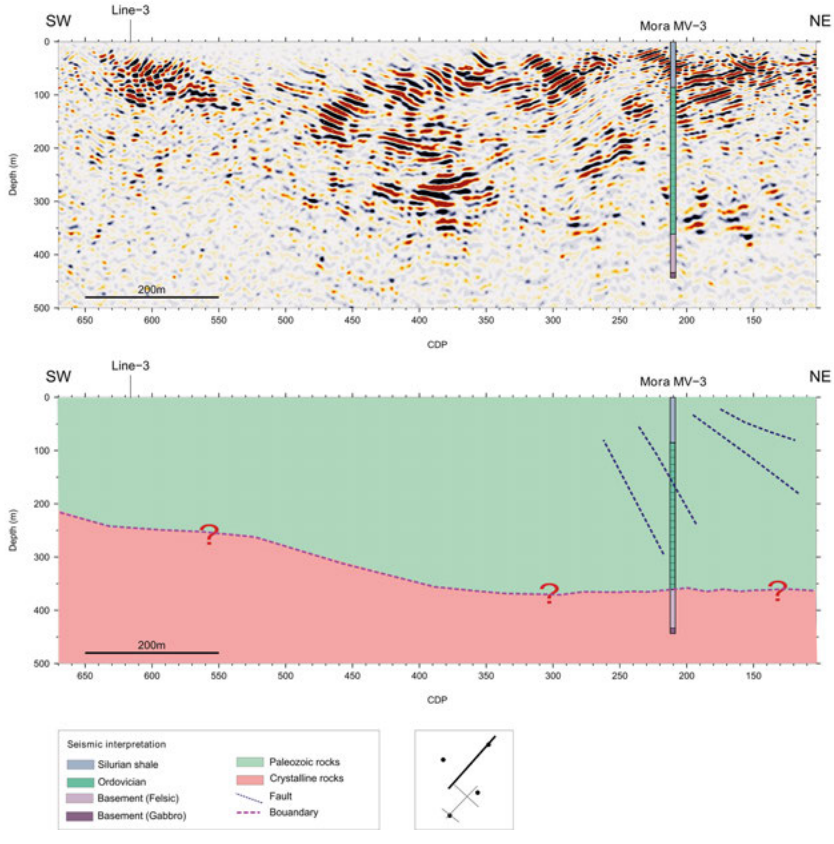

Figure 4.19 The upper image shows the final processed seismic depth section for Line 1. Core lithology of the Mora MV-3 well is annotated. The seismic interpretation, denoting the thickness of the Paleozoic sequence and the location of faults is shown in the lower image.

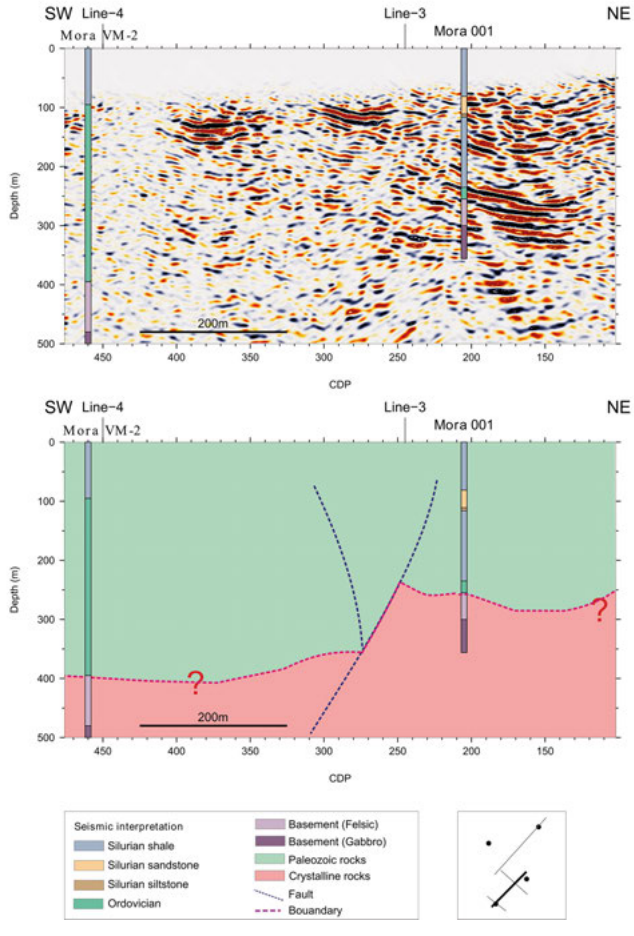

Figure 4.20 The upper image shows the final processed seismic depth section for Line 2. Core lithology of the Mora 001 and Mora VM-2 wells is annotated. The seismic interpretation, denoting the thickness of the Paleozoic sequence and the location of faults is shown in the lower image.

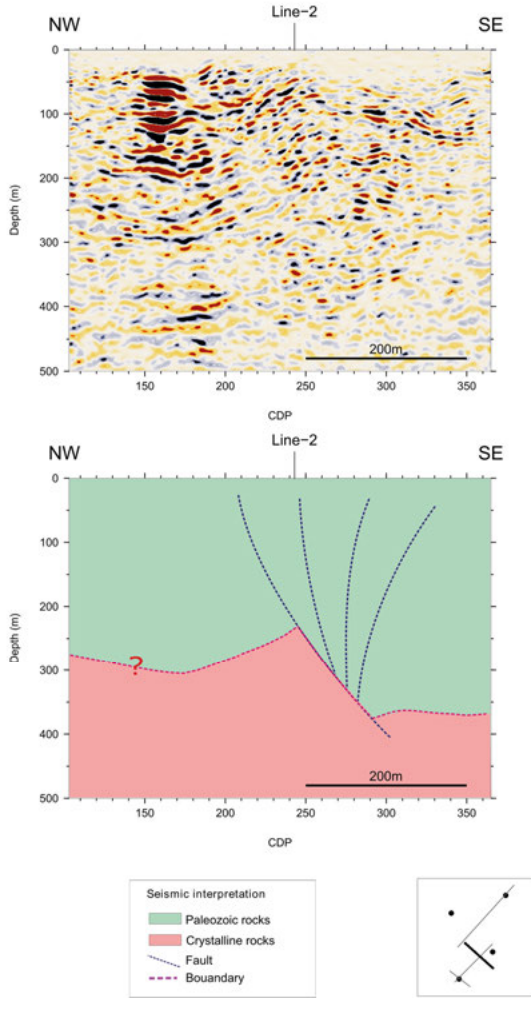

Figure 4.21 The upper image shows the final processed seismic depth section for Line 3. The seismic interpretation, denoting the thickness of the Paleozoic sequence and the location of faults is shown in the lower image.

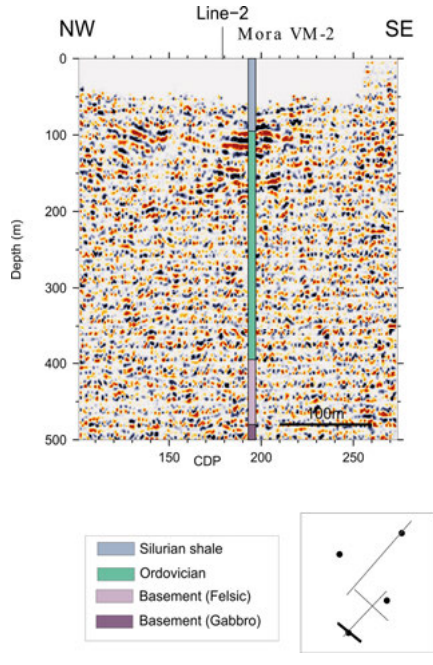

Figure 4.22 The final processed seismic depth section for Line 4. Core lithology of the Mora VM-2 well is annotated.

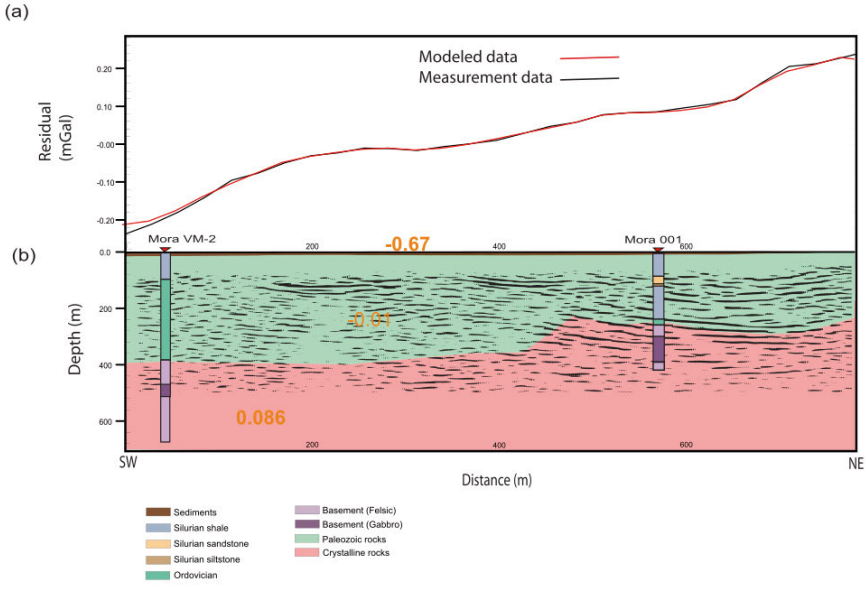

Figure 4.23 Gravity modeling along seismic Line 2, based on the interpretation of the seismic reflection data, density core samples and lithologies of the boreholes. (a) Gravity data and model response. (b) Integration of the seismic section and model based on the interpretation of the gravity data. The orange numbers in (b) represents the density contrast.

4.3.2 Conclusions

Four 2D high-resolution seismic reflection lines were acquired in the Mora area, with a total length about 3 km. The main objective was to study the Paleozoic successions in detail and map the sub-surface structure in the area. In addition, 42 sample of the Mora VM-2 core were taken from different lithologies, spread throughout the entire core, for the purpose of petrophysical data measurements. The laboratory measurements were made in the ultrasonic laboratory at Uppsala University. This petrophysical data were used to generate a synthetic seismogram to tie with the seismic sections for correlation purposes. Also, ground gravity (13 points) data were acquired along Line 2 and 2.5D density forward modeling was performed to help further constrain the seismic interpretation. The results of this study show highly deformed domains in areas of the southwestern Siljan ring structure. We are able to identify several distinct fault blocks with different levels of structural complexity. These fault blocks and the associated faults appear to be consistent between seismic lines.

5 Conclusions and outlook

5.1 Conclusions

The studies in this thesis focused on the western part of the Siljan Ring impact crater. Various geophysical techniques and petrophysical methods have been presented along with their integration and joint interpretation to study the sedimentary and crystalline basement rocks in this part of the Siljan Ring. Paper I and paper III focus on analysis of the down-hole logging data and borehole core data, as well as the acquisition, processing and interpretation of 2D high-resolution seismic reflection data from the Mora area. The aims were to determine several physical properties of the Paleozoic and crystalline rocks, in addition to mapping the Paleozoic successions and structure and to determine what faults might be present in the Mora area. The borehole log responses were compared with the core lithology of the Mora 001 borehole and information from two other cores (Mora VM-2 and Mora MV-3) in order to interpreted the logs. Furthermore, four 2D high-resolution seismic reflection profiles were designed to pass close to the boreholes in the Mora area. The seismic data acquisition was conducted using a 3C MEMs-based land streamer system combined with wireless units. The Uppsala University system is especially suitable for noisy urban or mining environments or areas where high-resolution images of the subsurface are needed.

The logging tools used included temperature, electrical and sonic sondes, all with a complimentary detector to measure the natural-gamma activity. The natural-gamma log response of the Mora 001 and Vattumyra Production boreholes were consistent with Mora 001 core lithology and this was used as a base to interpret the other borehole logs responses. The logs reveal significant changes in the lithology between boreholes, which we interpret as due to the complexity of the subsurface geology in the area related to impact tectonics. Furthermore, three key horizons with very high gamma readings were observed within the Ordovician limestones. The sonic log shows a high contrast in velocity between the Silurian and Ordovician successions. However, the log based velocity of the Ordovician limestones is higher than the velocity interpreted on the Mora seismic profile further to the north of the study area. In addition, the synthetic seismogram generated from the velocity log of the Mora 001 borehole shows a high amplitude reflection produced between the lower Silurian succession and the underlying Ordovician limestones.

Several thrust packages are identified in the wells in the Mora area. The apparent temperature gradient of 23–25 °C km^{-1} in the area is higher than the 16 °C km^{-1} recorded in the c. 6.5 km deep Gravberg-1 borehole in the northern part of the Siljan Ring (Juhlin, 1991). The higher temperature gradient in the study area may be due to the low thermal conductivity of the sedimentary rocks. This matter needs further investigation.

Additionally, the high-resolution 2D seismic data interpretations in the Mora area show that the area has been affected significantly by the impact. Petrophysical measurements on core from the Mora VM-2 borehole provided a basis to generate synthetic seismograms to tie with the seismic sections. Several potential faults were identified in the area and interpreted to be post depositional and related to the impact. Based on the seismic and well data we identify one relatively undeformed fault block, located in the northeastern side of Line 2 and on the northwestern part of Line 3. Here we interpret the Silurian rocks to be relatively thick. We interpret the increased thicknesses of the Ordovician rocks as due to thrusting in the area.

In paper II, we reprocessed the Orsa seismic profile in the northwestern part of the Siljan Ring. In addition, first break traveltime tomography, vintage seismic OPAB profiles, new and pre-existing gravity data, aeromagnetic data and the bedrock geological map were used to present a geological model along the profile. The reprocessing strategies were successful in boosting the signal in the data. Using the reprocessed profile and the interpreted OPAB data a simple geological model consistent with the surface geological map was constructed. There are two reflective horizons which have been interpreted in the seismic data. The upper reflection is interpreted to be the top of the Ordovician and the lower one to be the top of the basement. The traveltime results are generally consistent with the model, except in the northern part of the Orsa profile where high velocity material is found in the interpreted Silurian succession. The 2.5D gravity forward model provides a better match to the observed data than the magnetic model. Scientific drilling is required in the area to verify this interpretation.

5.2 Outlook

This research and the previous studies in the Siljan Ring structure show that the subsurface geology is very complex. Our research in the western part of the Siljan Ring has provided new information on the geological structures, but has also generated new questions. In the Mora and Orsa areas, more research needs to be performed. In the Mora area it will be very useful to carry out high-resolution 3D reflection seismic techniques with as long offset as possible to overcome 3D effects and better image the shallow subsurface. Since 3D seismic surveys are expensive if could be useful to perform a 3D gravity survey in the area first.

The high-resolution 2D seismic reflection data that were acquired in the Mora area include 3C (vertical, horizontal and radial components) data. In this research we only used the vertical component data and it is possible that analysis of the other components data will provide new information. Moreover, multi-component data analysis could be used to constrain the seismic interpretation and may allow information about anisotropic structures to be obtained. Furthermore, the S-wave arrivals can be picked on the full-waveform log of the Mora 001 borehole and compared to the horizontal seismic component data.

The temperature logs in the Mora area showed that the geothermal gradient in this area is higher than what was found in the northern part of the Siljan Ring (Juhlin, 1991). The high temperature gradient in the study area maybe due to the low thermal conductivity of the sedimentary rocks, but thermal modeling is important to study the issue in more detail.

In the Orsa area we had several geophysical data sets and the integration between them helped us in producing an integrated interpretation, but the lack of deep borehole information in the area made these interpretations uncertain. Therefore, scientific drilling to 800 m in the northern part of the Orsa seismic profile would investigate the hypothesis put forth and would also verify the presence of the graben structure seen on the reflection seismic data.

6 Summary in Swedish

I vårt solsystem återfinns nedslagstrukturer från meteoriter på alla himlakroppar som har en fast yta. För vår egen planet har 190 nedslagsstrukturer bekräftats till dags dato, 2017-01-12, vilka är dokumenterade i Earth Impact Database. Antal ökar för varje år. En nedslagskrater är en ungefär cirkelformad depression av jordens yta, som har formats genom att en mindre kropp i mycket hög hastighet har kolliderat med jordytan.

Siljanringens nedslagsstruktur är den största i Europa (Fig. 1.2). Den är belägen i mellersta Sverige (N 61^{o} 2', E 14^{o} 52') och är daterad till senare delen av devon. Siljanringen anses vara en komplex nedslagsstruktur. Diametern av nedslagsstrukturen före erosionen började nöta har uppskattats till 52 km utifrån seismiska studier (Grieve, 1988; Juhlin and Pedersen, 1993) och i ett område med en diameter på 65 km har sprickor från nedslaget dokumenterats i den kristallina berggrunden (Kenkmann and von Dalwigk, 2000a). Geomorfologisk data indikerar att den totala diametern är 75 km (Henkel and Aaro, 2005) medan den största diametern som nämns i litteraturen är 90 km (Holm et al., 2011). Siljanringen består av en central upplyftning som är 20-30 km i diameter, denna kringgärdas av en ringformad depression med sediment från nedre paleozoikum. De paleozoiska sedimenten har tack vare depressionen skyddats från erosion.

I denna avhandling har flera geofysiska metoder använts för att studera Siljanringens nedslagsstruktur, fokus har varit på de nordvästra och sydvästra områdena (see Fig. 1.2). Denna avhandlingen, och de tre artiklarna som den är baserad på, försöker kartera de paleozoiska bergarterna i den ringformade gravsänkan och att karaktärisera dess strukturer. Vidare undersöks den underliggande kristallina berggrunden. För att åstadkomma detta har reflektionsseismik, borrhålsloggning, seismisk tomografi, samt potentialfältsmetoder används och datan har analyserats tillsammans för att ge en integrerad tolkning.

Artikel I och III fokuserar på analys av borrhålsloggning och borrkärnor samt datainsamling, processering och tolkning av högupplöst 2D-reflektionsseismik från Mora-området. Syftet var att bestämma fysikaliska egenskaper av paleozoiska och kristallina bergarter. Vidare var syftet att kartera den paleozoiska stratigrafin och dess strukturer, samt att identifiera förkastningar i Mora-området. För tolkning av borrhålsloggar jämfördes den med karteringen

av borrkärnan från borrhålet "Mora 001" och information från två andra kärnor ("Mora VM-2" och "Mora MV-3"). Fyra högupplösta 2D-reflektionsseismikprofiler som tangerade Mora plannerades och genomfördes också.

De tre borrhålssonderna som användes var bestyckade med temperaturmätare, elektriska respektive soniska sensorer. Alla tre sonder har också en sensor för mätning av naturlig gammastrålning. Naturlig gamma från borrhålen "Mora 001" och "Vattumyra Produktionsborrhål" stämde med kärnkarteringen från "Mora 001" och användes för att tolka borrhålsloggarna från de andra borrhålen. Borrhålsloggarna visar att det är en märkbar lateral och vertikal variation av litologin. Vår tolkning är att det beror på den komplexa geologin i området och att detta är relaterat till nedslagstektonik. Den soniska borrhålsloggen påvisar stor skillnad i seismisk hastighet mellan den siluriska och ordoviciska stratigrafin. Dock är hastigheten från borrhålsmätningarna högre för ordoviciska kalkstenar här än vad den har tolkats att vara enligt en seismisk profil längre norr ut i Mora-området. I tillägg så visar ett syntetiskt seismogram från hastighetsloggen från borrhålet "Mora 001" att en kraftig reflektor kan förväntas från gränsen nedre silur och de där under liggande ordoviciska kalkstenarna.

Det finns flera geologiska enheter i Mora-området som vi har tolkat till att bestå av överskjutna block. Det verkar som samma block återfinns i borrhålen "Mora VM-2" och "Mora MV-3", men att det är andra block i de andra borrhålen. Temperaturgradienten är 23-25 °C/km i området vilket är högre än i det cirka 6,5 km djupa borrhålet "Gravberg-1" i den norra delen av Siljanringen där temperaturgradient har uppmätts till betydligt lägre 16 °C/km (Juhlin,1991). Den högre temperaturgradienten i det studerade området kan bero på lägre termisk konduktivitet i de sedimentära bergarterna. Detta behöver studeras vidare för att ge ett klart svar.

Tolkningen av den högupplösta 2D-reflektionsseismiken från Mora-området visar att området har påverkats märkbart av meteoritnedslaget. För att koppla samman geologin med de seismiska profilerna skapades syntetiska seismogram från petrofysiska mätningar på borrkärnor från borrhålet "Mora VM-2". Flera potentiella förkastningar identifierades i området och har tolkats att vara relaterade till meteoritnedslaget, dessa förkastningar är yngre än avsättningen sedimentbergarterna. Det finns två skenbart odeformerade block som visar sig i den seismiska datan, en sydöst om profil 2 och det andra nordväst om profil 3. Vi tolkar detta till att den siluriska sekvensen är mäktig i dessa områden. Vi tolkar vidare den ökade mäktigheten av den ordoviciska sekvensen kan vara orsakad av överskjutningar i området.

I artikel II presenterar vi resultaten från omprocessering av Orsa seismiska profil i den nordvästra delen av Siljanringen. I tillägg så används så kallad "first break traveltime"-tomografi, äldre seismiska profiler från OPAB, gammal och ny tyngdkraftdata, flygmagnetisk data och den berggrundsgeologiska kartor för att presentera en geologisk model längs den seismiska profilen. Metoden som användes vid omprocesseringen var framgångsrik i att förstärka

signalen i den seismiska datan. Med hjälp av den omprocesserade profilen och tolkningen av OPAB-datan skapades en enkel geologisk modell som stämmer överens med den karterade berggrundsgeologin på ytan. Det finns två tydliga reflektionshorisonter i den seismiska datan. Den övre reflektorn kommer enligt vår tolkning från toppen av ordovicium och den nedre kommer från överytan av den kristallina berggrunden. Gånghastigheterna stämmer i allmänhet väl överens med modelleringen, utom i den norra delen av Orsa-profilen där det är hög hastighet i vad som har tolkats som silurisk stratigrafi. 2.5D "forward"-modellering av tyngdkraft stämmer bättre överens med den observerade datan än motsvarande modellering av magnetisk data. Borrning är nödvändigt för att kunna bekräfta de här presenterade tolkningarna.

Acknowledgments

My great thanks to God for giving me strength and patience to perform this research, many people have contributed in various ways to the success of this work and as part of my appreciation to the contribution of those people I would like to express my profound gratitude to each of them.

Foremost, I would like to express my sincere gratitude to my main supervisor Prof. Christopher Juhlin for his undoubted support during my PhD study. He has been patient and very carefully keeping me on track with my research. I also appreciate him for giving me the opportunity to participate in fieldwork and attend conferences. I am very grateful for his patience, motivation, enthusiasm, and immense knowledge in geophysics that, taken together, make him a great mentor.

I am also very grateful to my assistant supervisor Prof. Alireza Malehmir who has offered quick response and valuable instructions. I cannot imagine a better and more supportive co-supervisor so thousands of thanks to him. Furthermore, I would like to thank Daniel Sopher, who has been my adviser over the last year of my PhD study for his immeasurable amount of support and guidance provided throughout the study.

I would like to thank Omid Ahmadi, the first person I met when I came to Uppsala. I want to appreciate him for his kindness when he picked me up in the central station and showed me different places in Uppsala. He helped me a lot to learn the Claritas software and seismic processing concepts. I would like to thank him again for all his endless support.

I want to acknowledge Hans Palm for his experience and immense knowledge in seismic fieldworks. I learned from him how fieldwork should be done, as well as how to use the DGPS device and plant geophones. Really, he will be missed. Magnus Andersson is especially thanked for his helps with down-hole logging measurements and gravity surveying. Also, Jockem is thanked for his help to collect rock samples from borehole core. I want to thank Bojan, Lars, Sara, Kristina and Mingkhwan for their help in the seismic fieldwork.

Many thanks to my office mates Karin, Ping, Ershad, Poua, George, Sadegh, Fei, Milad, View, Angeliki, Nawal, Abbas, Gardar, Michiel, Luisa, Lisa and schang. Thank you for the nice moments together and for all the talks we had. Throughout my work, I have learned greatly from and have been helped by the following colleagues: Omid, Magnus, Bojan, Daniel, Fengjiao, Peter, Fei, Silvia, Ping, Zeinab, Shunguo, Ari and Hamza. Thank you also to

all of the other PhD and Msc students, and the post-doc researchers which I have had the pleasure of working and sharing fika with throughout my study.

I would like to thank my co-authors, Christopher Juhlin, Alireza Malehmir, Daniel Sopher, Oliver Lehnert (Universität Erlangen, Germany, Tallinn University of Technology, Estonia, Lund University, Sweden), Guido Meinhold (Universität Göttingen, Germany), Magnus Anderson, Maria Garcia Juanatey and Arzu Arslan (Universität Göttingen, Germany) for collaborating with me and giving useful feedback on my work. Johan Michelsen (University of Bergen, Norway) is thanked for his constructive criticism on paper II.

I would like to thank Chris, Alireza, Daniel, Peter, Bojan, Magnus and Omid for reviewing this thesis and their comments. I want to especially thank Magnus Andersson for taking care of the Swedish summary of this thesis.

I would like to acknowledge Igrene AB Company for partly funding the seismic field work and providing some logistical support during the acquisition. Thanks to Andreas Gidlund and Mats Budh at Igrene AB for allowing access to the boreholes and for their support. The Geological survey of Sweden is thanked for providing gravity and magnetic data.

I would like to thank academic and support staff from the department of Earth Sciences. The Ministry of Education and Scientific Research in Iraqi Kurdistan Region is acknowledged for funding to study abroad.

I would like to thank Omid, Khalid, Azad, Araz, Revan and their families for sharing many wonderful moments and endless support. Many thanks are extended to my parents, sisters and brothers for their unconditional support and encouragement.

Last but not least, thanks to my wife, Rangeen, this work is as much hers as it is mine. Thanks for her support, help, encouragement and love. And also to my daughters Laveen and Nivin.

Harbe Muhamad, Uppsala, January 2017

References

Ahmadi, O., Juhlin, C., Malehmir, A. and Munck, M., 2013. High-resolution 2D seismic imaging and forward modeling of a polymetallic sulfide deposit at Garpenberg, central Sweden. Geophysics 78, B339-B350.

Allaud, L. A., and Martin, M. H., 1977. Schlumberger, the history of a technique, John Wiley and Sons, New York. 333 pp.

Arslan, A., Meinhold, G. and Lehnert, O., 2013. Ordovician sediments sandwiched between Proterozoic basement slivers: tectonic structures in the Stumsnäs 1 drill core from the Siljan Ring, central Sweden. GFF. 135, 213–227.

Birch, F., 1961. The velocity of compressional waves in rocks to 10 kilobars: 2. J. Geophys. Res. 66, 1083-1102. doi: 10.1029/JZ066i007p02199

Blakely, R. J., 1996. Potential theory in gravity and magnetic applications. Cambridge University Press.

Boden, A. and Eriksson, K.G., 1988. Deep Drilling in Crystalline Rock, in Vol.1 :The Deep Gas Drilling in the Siljan Impact Structure, Sweden and Astrobiemes , A. Boden and K.G. Eriksson (Eds.). Springer Verlag, Berlin, Germany, 364.

Brodic, B., Malehmir, A., Juhlin, C., Dynesius, L., Bastani, M. and Palm, H., 2015. Multicomponent broadband digital-based seismic landstreamer for near-surface applications, Journal of Applied Geophysics 123, 227-241.

Cella, F. and Fedi, M., 2012. Inversion of potential field data using the structural index as weighting function rate decay. Geophysical Prospecting 60(2), 313-336.

Collini, B., 1988. Geological Setting of the Siljan Ring Structure Deep Drilling in Crystalline Bedrock, in Vol.1: The Deep Gas Drilling in the Siljan Impact Structure, Sweden and Astrobiemes. Springer Verlag, Berlin, Germany, 349-354.

Dence, M.R., 1965. The extraterrestrial origin of Canadian craters, Annals of the New York Academy of Science 123, 941-969.

Donofrio, R.R., Olsen, K.H., Vlierboom, F.W., Witschard, F. and Petersson, G., 1984. Deep Gas, Swedish premises: the Siljan Ring project: independent expert evaluation. Stockholm, Vattenfall 63.

Eaton, D. W., Milkereit, B. and Salisbury, M. H. (Eds.), 2003. Hardrock seismic exploration. Geophysical Development Series 10, Society of Exploration Geophysicists.

Ebbestad, J.O.R. and Hogstrom, A.E.S., 2007. Ordovician of the Siljan district, Sweden. In J.O.R. Ebbestad, L.M. Wickstrom and A.E.S. Hogstrom (eds.): WOGOGOB 2007, 9th meeting of the Working Group on Ordovician Geology of Baltoscandia. Field guide and abstracts. Sveriges Geologiska Undersokning Rapporter och meddelanden 128, 7–26.

El-Batroukh, S.I. and Zentani, A.S., 1980. Gravity interpretation of Raguba field, Sirte basin, Libya. Geophysics 45 (7), 1153-1163.

French, B.M., 1998. Traces of Catastrophe. Handbook of Shock-Metamorphic Effects in Terrestrial Meteorite Impact Structures, Lunar and Planetary Institute, Houston, 1998.

Gault, D.E., Quaide, W.L. and Oberbeck, V.R., 1968. Impact cratering mechanics and structures, in: B.M. French, N.M. Short, (Eds), Shock Metamorphism of Natural Materials, Mono Book Corp., Baltimore, 87-99 pp.
Grahn, Y., 1998. Lower Silurian (Liandovery-Middle Wenlock) Chitinoza and biostratigraphy of the mainland of Sweden. GFF. 120, 273-283.
Grieve, R.A.F., 1988. The formation of large impact structures and constraints on the nature of Siljan, in Vol.1: The Deep Gas Drilling in the Siljan Impact Structure, Sweden and Astrobiemes, A. Boden and K.G. Eriksson (Eds.). Springer Verlag, Berlin, Germany, 328-348.
Grieve, R.A.E and Masaitis, V.L., 1994. The economic potential of terrestrial impact craters. International Geology Review 36, 105-151.
Henkel, H. and Aaro, S., 2005. Geophysical investigations of the Siljan impact structure -a short review, in: Impact Tectonics, Koeberl, Henkel, H. (Eds.), I. Springer Verlag, Berlin, Germany, 247–283.
Holm, S., Alwmark, C., Alvarez, W. and Schmitz, B., 2011. Shock barometry of the Siljan impact structure, Sweden. Meteoritics and Planetary Science 46, 1888–1909.
Hughes, S. W., 2005. Archimedes revisited: s faster, better, cheaper method of accurately measuring the volume of small objects. Phys. Educ. 40, 468-474. doi: 10.1088/0031-9120/40/5/008.
Jackson, I., Niesler, H. and Weidner, D. J., 1981. Explicit correction of ultrasonically determined elastic wave velocities for transducer-bond phase shifts. J. Geophys. Res., 86, 3736–3748.
Jourdan, F., Reimold, W.U., and Deutsch, A., 2012. Dating terrestrial impact structures. Elements 8, 49–53.
Juhlin, C., and Pedersen, L.B., 1987. Reflection seismic investigations of the Siljan impact structure, Sweden. Journal of Geophysical Research 92, 14113–14122.
Juhlin, C., 1990. Interpretation of the reflections in the Siljan Ring area based on results from the Grayberg-1 borehole. Tectonophysics 173, 345-360.
Juhlin, C., 1991. Scientific Summary Report of the Deep Gas Drilling Project in the Siljan Ring Impact Structure, Vattenfall FUD Report no. UG 1991(14).
Juhlin, C. and Pedersen, L. B., 1993. Further constraints on the formation of the Siljan impact crater from seismic reflection studies, Geologiska Föreningen i Stockholm Förhandlingar 115, 151-158.
Juhlin, C., 1995. Finite difference elastic wave propagation in 2-D heterogeneous transversely isotropic media. Geophysical Prospecting 43, 843–858.
Juhlin, C., Sturkell, E., Ebbestad, J.O.R., Lehnert, O., Hogstrom, A.E.S. and Meinhold, G., 2012. A new interpretation of the sedimentary cover in the western Siljan Ring area, central Sweden, based on seismic data. Tectonophysics 860, 88–99.
Kearey, P., Brooks, M. and Hill, I., 2002. An introduction to geophysical exploration. John Wiley and Sons, Oxford.
Kenkmann, T. and von Dalwigk, I., 2000a. Radial transpression ridges: a new structural feature of complex impact craters. Meteoritics and Planetary Science 35, 1189–1202.
Keys, W.S., 1990. Borehole geophysics applied to ground-water investigations: U.S. Geological Survey Techniques of Water-Resources Investigation, book 2, chap. E2, 150 pp.
Khan, K. A., 2010. Geophysical techniques for exploration of natural resources. Oil and Gas Training Institute (OGDCL), Islamabad Pakistan.
Kresten, P., Aaro, S., and Karis, L., 1992. Latest results of bedrock mapping in the Siljan area, in D. G., Gee (Eds.), Geol. Fören. Stockholm Förh. 114, 155–164.

Larner, K. L., Gibson, B. R., Chambers, R. and Wiggins, R. A., 1979. Simultaneous Estimation of Residual Static and Cross-dip Corrections. Geophysics 44, 1175-1192.

Lehnert, O., Meinhold, G., Bergstrom, S.M., Calner, M., Ebbestad, J.O.R., Egenhoff, S., Frisk, A.M., Hannah, J.L., Hogstrom, A.E.S., Huff, W.D., Juhlin, C., Maletz, J., Stein, H.J., Sturkell, E. and Vandenbroucke, T.R.A., 2012. New Ordovician–Silurian drill cores from the Siljan impact structure in central Sweden: an integral part of the Swedish Deep Drilling Program. GFF. 134, 87 –98.

Li, Y. and Oldenburg, D. W., 1998. Separation of regional and residual magnetic field data. Geophysics 63, 431–439.

Malehmir, A., Tryggvason, A., Lickorish, H. and Weihed, P., 2007. Regional structural profiles in the western part of the Palaeoproterozoic Skellefte Ore District, northern Sweden. Precambrian Research 159, 1–18.

Malehmir, A., Thunehed, H. and Tryggvason, A., 2009. The Paleoproterozoic Kristineberg mining area, northern Sweden: results from integrated 3D geophysical and geological modeling, and implications for targeting ore deposits. Geophysics 74, B9–B22.

Malehmir, A., Durrheim, R., Bellefleur, G., Urosevic, M., Juhlin, C., White, D., Milkereit, B., and Campbell, G., 2012. Seismic methods in mineral exploration and mine planning: A general overview of past and present case histories and a look into the future. Geophysics, 77, WC173–WC190.

Malehmir, A., Andersson, M., Lebedev, M., Urosevic, M. and Mikhaltsevitch, V., 2013. Experimental estimation of velocities and anisotropy of a series of Swedish crystalline rocks and ores. Geophys. Prospect. 61, 153-167. doi: 10.1111/j.13652478.2012.01063.x

Malehmir, A., Wang, S., Lamminen, J., Brodic, B., Bastani, M., Vaittinen, K., Juhlin, C., and Place, J., 2015a. Delineating structures controlling sandstone-hosted base-metal deposits using high-resolution multicomponent seismic and radio-magnetotelluric methods: a case study from Northern Sweden. Geophysical Prospecting, 63, 774–797.

Malehmir, A., Zhang, F., Dehgahnnejad, M., Lundberg, E., Döse, C., Friberg, O., Brodic, B., Place, J., Svensson, M., and Möller, H., 2015b. Planning of urban underground infrastructure using a broadband seismic landstreamer—Tomography results and uncertainty quantifications from a case study in southwest of Sweden. Geophysics, 80, B177–B192.

Malehmir, A., Andersson, M., Mehta, S., Brodic, B., Munier, R., Place, J., Maries, G., Smith, C., Kamm, J., Bastani, M., Mikko, H., and Lund, B., 2016. Post-glacial reactivation of the Bollnäs fault, central Sweden - a multidisciplinary geophysical investigation. Solid Earth, 7, 509–527.

Malehmir, A., Heinonen, S., Dehgahnnejad, M., Heino, P., Maries, G., Karell, F., Suikkanen, M., and Salo, A., 2017. Landstreamer seismics and physical property measurements in the Siilinjärvi open-pit apatite (phosphate) mine, central Finland. Geophysics. doi: 10.1190/GEO2016-0443.1

Maries, G., Ahokangas, E., Mäkinen, J., Pasanen, A., and Malehmir, A., 2017. Interlobate esker architecture and related hydrogeological features derived from a combination of high-resolution reflection seismics and refraction tomography, Virttaankangas, SW-Finland. Hydrogeology Journal. doi: 10.1007/s10040-016-1513-9

Muhamad, H., Juhlin, C., Lehnert, O., Meinhold, G., Andersson, M., Garcia Juanatey, M. and Malehmir, A., 2015. Analaysis of borehole geophysical data from the Mora area of the Siljan Ring impact structure, central Sweden. Journal of Applied Geophysics 115, 183-196. doi: 10.1016/j.jappgeo.2015.02.019

Masaitis, V. L., 1989. The economic geology of impact craters. International Geology Reviews 31, 922-933.
Nabighian, M. N., Ander, M. E., Grauch, V. J. S., Hansen, R. O., LaFehr, T. R., Li, Y., Pearson, W. C., Peirce, J. W., Phillips, J. D. and Ruder, M. E., 2005. Historical development of the gravity method in exploration. Geophysics 70, 63–89.
Nedimovic, M.R. and West, G.F., 2003. Crooked line 2D seismic reflection imaging in crystalline terrains: Part 1, data processing. Geophysics 68, 274-285.
Nettleton, L. L., 1976. Gravity and Magnetic in Oil Prospecting. McGraw-Hill Book Co.
Osinski, G.R., 2004. Hypervelocity impacts into sedimentary targets: Processes and products, PhD Thesis, University of New Brunswick.
Özbek, A., 2000. Adaptive beamforming with generalized linear constraints. Geophysics Extended Abstract, Society of Exploration Geophysicists.
Papasikas, N. and Juhlin, C., 1997. Interpretation of reflections from the central part of the Siljan Ring impact structure based on results from the Stenberg-1 borehole. Tectonophysics 269, 237-245.
Podvin, P. and Lecomte, I., 1991. Finite different computation of traveltimes in very contrasted velocity models: Amassively parallel approach and its associated tools. Geophysical Journal International 105, 271–284.
Pratt, R.G. and Worthington, M.H., 1990. Inverse theory applied to multi-source cross-hole tomography. Part I: acoustic wave-equation method. Geophys. Prospect. 38, 287–310.
Rawlinson, N. and Sambridge, M., 2003b. Seismic traveltime tomography of the crust and lithosphere. Adv. Geophys. 46, 81–198.
Reimold, W.U., Kelley, S.P., Sherlock, S., Henkel, H. and Koeberl, C., 2005. Laser argon dating of melt breccias from the Siljan impact structure, Sweden: implications for a possible relationship to late Devonian extinction events. Meteoritics and Planetary Science 40, 591–607.
Reimold, W.U., Koeberl, C., Gibson, R.L. and Dressler, B.O., 2005b. Economic mineral deposits in impact structures; a review. In C. Koeberl and H. Henkel (eds.): Impact tectonics, 479– 522. Springer Verlag, Berlin.
Reynolds, J., 2011. Introduction to Applied and Environmental Geophysics. Wiley-Blackwell.
Salisbury, M., Harvey, CW. and Matthews, L., 2003. The acoustic properties of ores and host rocks in hardrock terranes. In: Hardrock Seismic Exploration, Eaton, D., Milkereit, B. and Salisbury, M. Edited by Eaton, D., Milkereit, B. and Salisbury, M., SEG Developments in Geophysics series 10, 9-19.
Salisbury, H.M., Milkereit, B., Ascough, G., Adair, R., Matthews, L., Schmitt, DR, Mwenifumbo, J., Eaton, DW. and Wu, J., 2000. Physical properties and seismic imaging of massive sulfides. Geophysics 65, 1882-1889.
Shearer, P. M., 1999. Introduction to seismology. Cambridge, Cambridge University Press.
Sheriff, R. E. and Gerald, L. P., 1995. Exploration Seismology, Cambridge Univ. Press, Second edition, 592 pp.
Sopher, D., 2016. Characterization of the structure, stratigraphy and CO2 storage potential of the Swedish sector of the Baltic and Hanö Bay basins using seismic reflection methods. Digital Comprehensive Summaries of Uppsala Dissertations from the Faculty of Science and Technology 1355. 85 pp. Uppsala: Acta Universitatis Upsaliensis. ISBN 978-91-554-9515-2.

Stanchits, S., Vinciguerra, S. and Dresen, G., 2006. Ultrasonic velocities, Acoustic Emission Characteristics and Crack Damage of Basalt and Granite. In: Dresen G, Zang A, Stephansson O. (eds) Rock Damage and Fluid Transport, Part I. Birkhäuser Basel, 975-994.

Steeples, D.W. and Miller, R.D., 1998. Avoiding pitfalls in shallow seismic reflection surveys. Geophysics 63, 1213-1224.

Tryggvason, A. and Bergman, B., 2006. A traveltime reciprocity discrepancy in the Podvin and Lecomte time 3d finite difference algorithm. Geophysical Journal International 165, 432–435.

Tryggvason, A., Rognvaldsson, S.Th. and Flovenz, O.G., 2002. Three-dimensional imaging of the P- and S-wave velocity structure and earthquake locations beneath Southwest Iceland. Geophysical Journal International 151, 848–866.

Ulrych, T. J., Sacchi, M. D., and Graul, J. M., 1999. Signal and noise separation: Art and science. Geophysics 64, 1648- 1656.

Vanorio, T., Prasad, M., Patella, D. and Nur, A., 2002. Ultrasonic velocity measurements in volcanic rocks: correlation with microtexture. Geophys. J. Int. 149, 22-36. dio: 10.1046/j.0956-540x.2001.01580.x

Vidale, J., 1988. Finite-difference calculation of travel times. Bulletin of the Seismological Society of America 78, 2062–2076.

Westbroek, H. H. and Stewart, R. R., 1996. The formation, morphology, and economic potential of meteorite impact craters. CREWES Research Report 8, 1–26.

Wickman, F.E., 1981. Displacements and the Siljan ring structure. Geographiska Annaler, 63A, 313 –317.

Wu, J., Milkereit, B. and Boerner, D. E., 1995. Seismic imaging of the enigmatic Sudbury Structure. Journal of Geophysical Research 100, 4117-4130.

Wu, J., 1996. Potential pitfalls of crooked-line seismic reflection surveys. Geophysics 61, 277-281. doi: 10.1190/1.1443949

Xu, Y., Hao, T., Li, Z., Duan, Q. and Zhang, L., 2009. Regional gravity anomaly separation using wavelet transform and spectrum analysis. Geophysics and Engineering 6 (3), 279-287.

Yilmaz, Ö., 1989. Seismic data processing. Society of Exploration Geophysics (SEG), Tulsa.

Yilmaz, Ö., 2001. Seismic Data Analysis: Processing, Inversion, and Interpretation of Seismic Data. Society of Exploration Geophysicists

Zelt, C.A., Ellis, R.M. and Zelt, B.C., 2006. 3-D structure across the Tintina strike-slip fault, northern Canadian Cordillera, from seismic refraction and reflection tomography. Geophys. J. Int. 167, 1292–1308.

Acta Universitatis Upsaliensis

Digital Comprehensive Summaries of Uppsala Dissertations from the Faculty of Science and Technology 1468

Editor: The Dean of the Faculty of Science and Technology

A doctoral dissertation from the Faculty of Science and Technology, Uppsala University, is usually a summary of a number of papers. A few copies of the complete dissertation are kept at major Swedish research libraries, while the summary alone is distributed internationally through the series Digital Comprehensive Summaries of Uppsala Dissertations from the Faculty of Science and Technology. (Prior to January, 2005, the series was published under the title "Comprehensive Summaries of Uppsala Dissertations from the Faculty of Science and Technology".)

Distribution: publications.uu.se
urn:nbn:se:uu:diva-312022

ACTA
UNIVERSITATIS
UPSALIENSIS
UPPSALA
2017